

Dynamical transitions from slow to fast relaxation in random open quantum systems

Dror Orgad¹, Vadim Oganessian^{2,3}, and Sarang Gopalakrishnan⁴

¹*Racah Institute of Physics, The Hebrew University, Jerusalem 91904, Israel*

²*Department of Physics and Astronomy, College of Staten Island, CUNY, Staten Island, NY 10314, USA*

³*Center for Computational Quantum Physics, Flatiron Institute, 162 5th Avenue, New York, NY 10010, USA*

⁴*Department of Electrical and Computer Engineering, Princeton University, Princeton, NJ 08540, USA*

We explore the effects of spatial locality on the dynamics of random quantum systems subject to a Markovian noise. To this end, we study a model in which the system Hamiltonian and its couplings to the noise are random matrices whose entries decay as power laws of distance, with distinct exponents α_H, α_L . The steady state is always featureless, but the rate at which it is approached exhibits three phases depending on α_H and α_L : a phase where the approach is asymptotically exponential as a result of a gap in the spectrum of the Lindblad superoperator that generates the dynamics, and two gapless phases with subexponential relaxation, distinguished by the manner in which the gap decreases with system size. Within perturbation theory, the phase boundaries in the (α_H, α_L) plane differ for weak and strong decoherence, suggesting phase transitions as a function of noise strength. We identify nonperturbative effects that prevent such phase transitions in the thermodynamic limit.

The dynamics of generic quantum systems has been a central theme in contemporary many-body physics, spanning disciplines from quantum information to condensed matter and high-energy physics. A key conceptual tool in this context is random matrix theory (RMT), which prescribes studying systems governed by dynamics that is as random as is allowed by the symmetries and other constraints of the underlying problem of interest. RMT has been used over the past four decades to study quantum chaos in closed systems that lack spatial structure [1, 2]. Recently, various extensions of RMT that include forms of spatial structure were considered. These range from banded random matrices [3] (which represent generic local *single-body* problems), to random circuits [4] (which represent random many-body problems with no structure beyond the spatial locality of interactions), and the SYK model [5] (in which interactions are *few-body* but not otherwise local). Such explorations have led to a deeper understanding of quantum chaos, entanglement dynamics, and related questions.

Despite some early applications of RMT to *open* quantum systems [6–9], studies of systems whose Hamiltonian and couplings to a Markovian bath are drawn from RMT ensembles have only recently appeared [10–22]. A notable conclusion that has emerged is that such fully nonlocal open systems are rapidly equilibrating, i.e., the spectrum of their Lindblad superoperator is generically *gapped* in the thermodynamic limit. This conclusion is supported by numerical evidence, exact solutions, and general bounds [12, 13]. In contrast, one does not expect a gap in the opposite limit of local dissipative dynamics where the slowest-relaxing modes are long-wavelength spatial probability fluctuations, which decay through diffusion. For many-body systems with few-body interactions, the connectivity graph is more complicated but is still local in Fock space, hence suggesting a gapless Lindbladian, consistent with numerics [16]. The discrepancy

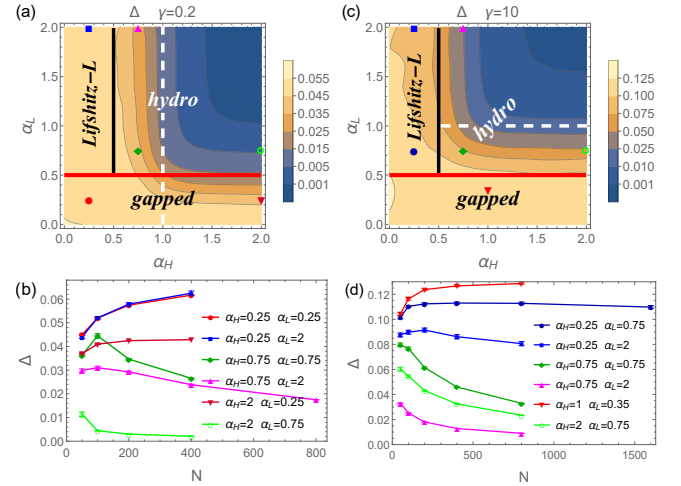


FIG. 1. (a) The Lindbladian spectral gap as function of the exponents α_H, α_L at weak decoherence $\gamma = 0.2$ and $N = 100$. The solid lines mark the $N \rightarrow \infty$ phase transitions between gapped, hydrodynamic, and Lifshitz phases. The dashed line marks a change in the populations content of the slowest decaying eigenvector. (b) N -dependence of the gap for selected values of (α_H, α_L) indicated by colored symbols in (a). (c)-(d) Similar data at strong decoherence $\gamma = 10$.

between the local and nonlocal regimes indicates that there must be a phase transition between them.

In this work we identify such phase transitions by exploring an ensemble of master equations constructed from power-law random banded matrices (PRBMs). PRBMs can be regarded as random hopping models in one dimension, with hopping that falls off as a power α of the distance between two sites [3, 23–25]. They interpolate between conventional random matrices in the $\alpha \rightarrow 0$ limit and short-range hopping systems with power-law localized eigenvectors for large α . These models have been studied extensively in the Hamiltonian case [3], where a

localization transition occurs at $\alpha = 1$. Here, we analyze related ensembles for *open* systems, whose Hamiltonian and couplings to a Markovian noise of strength γ are given by $N \times N$ PRBMs with two distinct powers α_H and α_L . We find a rich phase diagram, shown in Fig. 1, containing three dynamical phases: (i) a gapped phase in which the relaxation rate remains independent of N , (ii) a “hydrodynamic” phase where the relaxation rate falls off as a power law of N and the slowest-relaxing modes are long-wavelength fluctuations, and (iii) a “Lifshitz” phase where the relaxation rate falls off logarithmically in N , and the slowest-relaxing modes are localized perturbations in real space. Notably, we find that the limits $N \rightarrow \infty$ and $\gamma \rightarrow 0$ (or $\gamma \rightarrow \infty$) do not always commute, and finite- N systems with given (α_H, α_L) may exhibit quite different behaviors for small and large γ . However, we show that in the $N \rightarrow \infty$ limit the weak- and strong-decoherence regimes connect smoothly and any phase transitions as a function of γ (apart from the appearance of mid-gap states reported for the pure RMT case [12]) are avoided due to nonperturbative effects.

Model.—We consider systems described by noisy dynamics of the form $H(t) = H + \xi(t)L$, where ξ is a Gaussian Markovian noise with variance γ . The Hamiltonian H and the jump operator L are $N \times N$ random matrices [26], whose elements in the position basis are $G_{ij}f_{ij}$. Here, G is a matrix from the Gaussian orthogonal ensemble and $f_{ij} = 1/(\delta_{ij} + |i - j|^\alpha)$, where the exponent α generally takes different values, α_H and α_L , for H and L . We normalize G such that the variance of the spectrum of both H and L is $1/2$ for all α_H, α_L . The noise-averaged dynamics is described by the Lindblad master equation

$$\partial_t \rho = \mathcal{L} \rho \equiv -i[H, \rho] + \gamma(L\rho L - L^2\rho/2 - \rho L^2/2). \quad (1)$$

The eigenvalues of the Lindbladian superoperator \mathcal{L} occupy the complex half-plane $\text{Re}(\lambda) \leq 0$ and are either real or form complex conjugated pairs [12]. The steady state ($\lambda = 0$) of the specified model is always the maximally mixed state $\rho_0 = \mathbb{I}/N$. The remaining right eigenvectors of \mathcal{L} are traceless matrices, ρ_i , $i = 1, \dots, N^2 - 1$, that are either Hermitian or form Hermitian conjugated pairs. A general density matrix can be expanded as $\rho(t) = \rho_0 + \sum_{i=1}^{N^2-1} (a_i e^{\lambda_i t} \rho_i + \text{H.c.})$ and its late-time approach to ρ_0 is governed by the eigenvalue with the smallest negative real part, $-\Delta$, and its corresponding eigenvector ρ_1 . (This is always true in finite systems, but important exceptions exist in the thermodynamic limit [27–29].) As $N \rightarrow \infty$, Δ may tend to a positive value (i.e., is “gapped”) or approach zero (“gapless”), and we compute its dependence on α_H , α_L , and γ .

Overview of PRBMs.—We will invoke the spectral properties of PRBMs and thus briefly review their properties [3, 30]. (i) For $\alpha < 1/2$, PRBMs are akin to structureless random matrices: their eigenstates are random vectors and their eigenvalues follow a Wigner semicircle

distribution. (ii) For $1/2 < \alpha < 1$, almost all eigenstates $|v\rangle$ are extended, as revealed by their inverse participation ratio (IPR) $I = \sum_{i=1}^N |v_i|^4$ that vanishes in the large- N limit. However, they typically exhibit sparse spatial structure spanning only a fraction of the sites. Concomitantly, the eigenvalue distribution becomes unbound due to Gaussian tails [25] consisting of states that are localized around potential extremes and are unable to find any resonances within the system. These tail states are subextensive in number but, as we will show, may dominate the late-time dynamics. (iii) For $\alpha > 1$, all eigenstates are localized with power-law decay $|v_i| \sim 1/i^\alpha$.

Rate equations: small γ .—We begin by discussing the limit of small or large γ at finite N , where the analysis is facilitated by the ability to perturbatively eliminate all but N of the eigenvectors of \mathcal{L} . As noted above, the limits $\gamma \rightarrow 0, \infty$ and $N \rightarrow \infty$ do not always commute and we will address this issue later on. Consider first the case $\gamma = 0$. Here, the eigenvectors of \mathcal{L} are $|ij\rangle \equiv |i\rangle\langle j|$ with eigenvalues $i(E_i - E_j)$, where $H|i\rangle = E_i|i\rangle$. The N eigenvectors of the form $|ii\rangle$ have zero eigenvalue, i.e., are steady states. Following the convention in the NMR literature we dub them “ H -populations” and the other $N(N - 1)$ states “ H -coherences”. At first order in γ the noise does not couple populations and coherences, and one can write down classical rate equations for the populations [12], $\partial_t |ii\rangle = \sum_j A_{ij} |jj\rangle$, where

$$A_{ij} = \gamma(|\langle i|L|j\rangle|^2 - \delta_{ij}\langle i|L^2|j\rangle). \quad (2)$$

When $\alpha_H < 1/2$, the eigenbasis of H is effectively random, leading to rates A_{ij} that are approximately chi-squared distributed with a mean and a standard deviation that scale as γ/N . We have previously shown that such conditions lead to a gap $\Delta = \gamma/2$ [12]. Conversely, when $\alpha_H > 1$ the H -eigenvectors are localized. Analytical progress can be made by modeling them as a set of power-law envelopes centered on each of the N sites (ignoring their mutual orthogonality) and by averaging A_{ij} over the statistics of L . Within this “mean-field” approximation A is similar to a Hamiltonian whose hopping amplitudes between sites i, j vary as $|i - j|^{-2\alpha'}$, where $\alpha' \equiv \min(\alpha_H, \alpha_L)$, and whose rows sum up to zero [30]. The mean-field analysis predicts a gap when $\alpha' < 1/2$, a superdiffusive relaxation for $1/2 < \alpha' < 3/2$ with a lowest eigenvalue that vanishes as $N^{1-2\alpha'}$, and diffusive dynamics where this eigenvalue vanishes as N^{-2} for $\alpha' > 3/2$. Solving the rate equations numerically yields a qualitatively similar behavior with a gapped phase for $\alpha_L < 1/2$ and a gapless phase for $\alpha_L > 1/2$, albeit with a slower decay of the lowest eigenvalue with N as compared to the mean-field prediction [30]. For $1/2 \leq \alpha_H \leq 1$ the typical eigenstates of H do not have a simple description. Our numerical results indicate a gapped phase for $\alpha_L < 1/2$ and a “weakly gapless” behavior for $\alpha_L > 1/2$, where ρ_1 is a localized population in the Lifshitz tail of H whose eigenvalue slowly decreases with N [30].

Rate equations: large γ .—A similar analysis can be carried out at large γ [12]. Here, one begins by diagonalizing the dissipative part of \mathcal{L} , finding eigenvectors of the form $|\mu\nu\rangle = |\mu\rangle\langle\nu|$, with eigenvalues $-(\gamma/2)(\kappa_\mu - \kappa_\nu)^2$, where $L|\mu\rangle = \kappa_\mu|\mu\rangle$. Again, there are N eigenvectors with zero eigenvalue corresponding to “ L -populations”. Eliminating their coupling to the remaining $N(N-1)$ “ L -coherences” to second-order in H leads to rate equations $\partial_t|\mu\mu\rangle = \sum_\nu A_{\mu\nu}|\nu\nu\rangle$ with transition rates

$$A_{\mu\nu} = \frac{4}{\gamma} \frac{|\langle\mu|H|\nu\rangle|^2(\kappa_\mu - \kappa_\nu)^2}{(\kappa_\mu - \kappa_\nu)^4 + (2/\gamma)^2(\langle\mu|H|\mu\rangle - \langle\nu|H|\nu\rangle)^2}. \quad (3)$$

Probability conservation enforces $A_{\mu\mu} = -\sum_{\nu \neq \mu} A_{\mu\nu}$. In the strict large- γ limit at finite N , one would ignore the γ -dependent part of the denominator. However, this term regularizes the effective dynamics for all finite γ . Hence, we discuss Eq. (3) below and contrast it with the unregularized form in the supplemental material [30].

When $\alpha_L < 1/2$, the spectrum of L is *bounded* with extended states, causing H to act as a featureless random perturbation between L -populations. Consequently, one can coarse-grain Eq. (3) in κ -space and replace $|\langle\mu|H|\nu\rangle|^2$ by its average to find a gap $\Delta \simeq 2/\gamma$ [12, 30]. For $1/2 < \alpha_L < 1$, most of the L -eigenvectors are still delocalized. However, typical realizations of L also have spatially-localized tail states whose eigenvalues are far from the rest of the spectrum of L . The matrix elements out of these tail states are suppressed according to Eq. (3). As a rough estimate, in a sample of size N the extremal eigenvalue resides approximately $\sqrt{\log N}$ away from the bulk of the spectrum [30]. ρ_1 is localized on this extremal state, and the gap closes logarithmically in system size. When $\alpha_L > 1$ the eigenvectors of L are localized and its spectrum is unbounded. Consider the case $\alpha_L = \infty$, where they are roughly localized on sites and the dominant dependence of $A_{\mu\nu}$ comes from $|\langle\mu|H|\nu\rangle|^2$, scaling as $|\mu - \nu|^{-2\alpha_H}$. For $\alpha_H < 1/2$, these elements fluctuate sufficiently weakly that one can still coarse grain [30]. Since the L -spectrum is unbounded, tail states set a logarithmically decaying gap. For $\alpha_H > 1/2$ the effective hopping between L -populations is local, leading to hydrodynamic behavior with extended eigenvectors and a gap that decays as a power-law with N . Numerically, we find that this behaviour persists down to $\alpha_L = 3/2$, where the gap is again set by tail states [30].

Comparison of small and large γ .—We briefly summarize our findings using the rate equations. (a) When $\alpha_L < 1/2$, a gapped phase is predicted for all γ . (b) When α_H, α_L are both sufficiently large ($\alpha_H > 1, \alpha_L > 3/2$), a gapless phase is predicted for all γ . (c) Elsewhere, the rate equations for small and large γ yield incompatible results. For $\alpha_H < 1/2, \alpha_L > 1/2$ they suggest a gap-closing transition at finite γ , and in the remaining part of the (α_H, α_L) plane they disagree on the way the gap closes with increasing N . As we will argue, these discrepancies are absent for sufficiently large N .

Numerical investigation of \mathcal{L} .—We have contrasted the above predictions against the spectrum of the full Lindbladian (which is an $N^2 \times N^2$ matrix) for a relatively small system size $N = 100$, where a fine sweep across parameter space is feasible. We then examined larger systems of up to $N = 1600$ at selected points in the (α_H, α_L) plane. At these sizes, we do not have access to the full spectrum of \mathcal{L} but we can find the leading two eigenvalues and their corresponding eigenvectors by the power method. The resulting phase diagrams (Fig. 1) match our expectations from the rate equations in regimes (a) and (b) specified above. In regime (c), we find behavior that lies beyond the rate equations.

A more sensitive probe than the gap is the nature of ρ_1 . In the gapless regime we find that for small γ and N it follows the prediction of the rate equations and is extended both in the position and H eigenbases as long as $\alpha_H > 1$, while it is localized in both bases for $1 > \alpha_H > 1/2$ [30]. However, as N increases ρ_1 becomes delocalized in the entire $\alpha_H > 1/2$ gapless regime. One can characterize the failure of the rate equations by the fraction of the operator norm of ρ_1 that lies in the populations subspace. This is representing how well a population-only approximation (i.e., classical rate equation) can capture ρ_1 . As shown by supplemental Fig. 4 [30] the overlap with the populations is large for $\alpha_H > 1$, but diminishes with N for $\alpha_H < 1$. Intuitively, one expects such behavior if ρ_1 is hydrodynamic at large N , with a population that is modulated *in real space*. Since the eigenstates of H are delocalized when $\alpha_H < 1$, the projectors onto them miss the real-space structure. By contrast, for $\alpha_H > 1$ the eigenstates are localized, so local populations in energy space are a good proxy for local populations in real space.

We now support this intuition by analyzing the case $\gamma \ll 1, \alpha_L = \infty, 1/2 < \alpha_H < 1$, corresponding to a system subject to local noise and a Hamiltonian with power-law hopping and random on-site potentials. Consider a wavepacket initially localized in real space. In the clean system, it hybridizes via coherent tunneling with states at all distance scales R , with a Rabi frequency $\sim R^{-\alpha_H}$. However, local noise of strength γ sets a timescale γ^{-1} and a length-scale $R_\gamma \sim \gamma^{-1/\alpha_H}$ beyond which coherent tunneling is disrupted. For $R > R_\gamma$ transport is governed by incoherent hopping processes with a rate that is set by Fermi’s Golden Rule and scales as $1/R^{2\alpha_H}$. Since $2\alpha_H > 1$, incoherent hopping is *local* in this regime and the slow modes are accordingly hydrodynamic in real space. The eigenstates of H are the wrong basis because they are formed by delicate tunneling resonances that any amount of decoherence can disrupt. Evidently this argument extends to general $\alpha_L > 1$, and an exactly parallel argument can be made for large γ and $1/2 < \alpha_L < 1$.

ρ_1 remains delocalized for $\alpha_H > 1/2$ also in the strong-decoherence thermodynamic limit. This is apparent from Fig. 2, showing its IPR in the L -population subspace $\text{IPR}_L = \sum_\kappa \rho_{\kappa\kappa}^4 / (\sum_\kappa \rho_{\kappa\kappa}^2)^2$, where $\rho_{\kappa\kappa}$ are its components

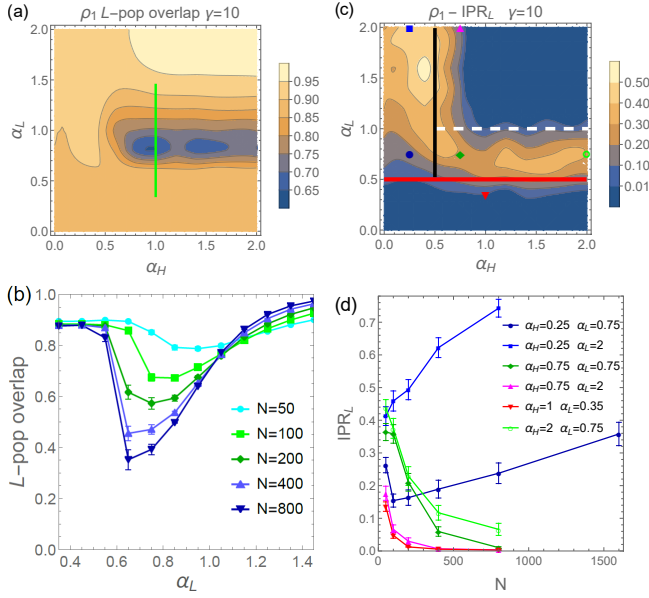


FIG. 2. (a) Overlap between ρ_1 and the L -populations at strong decoherence $\gamma = 10$ and $N = 100$. (b) N -dependence of the overlap along the cut shown in (a). L -coherences are essential to describe the state when $\alpha_H > 1/2$ and $1 > \alpha_L > 1/2$. (c) The IPR of ρ_1 in the L -eigenbasis. (d) N -dependence of the IPR for the (α_H, α_L) values indicated in (c). ρ_1 is dominated by a tail L -population when $\alpha_H < 1/2$, $\alpha_L > 1/2$.

within this subspace. Conforming to the prediction of the rate equations, the crossover regime $\alpha_H > 1/2$, $1 > \alpha_L > 1/2$ exhibits an eigenvector that is still largely concentrated on a population of a spatially-localized L -tail state at small N . However, the IPR_L diminishes with N , and ρ_1 becomes modulated in real space. Hence, for similar reasons to those outlined above its projection onto the L -populations also vanishes, see Fig. 2. In contrast, the IPR_L increases with N when $\alpha_H < 1/2$, $\alpha_L > 1/2$. We have confirmed that this is a result of ρ_1 becoming more concentrated on a population of a localized L -tail state. Thus, we conclude that the range $\alpha_H < 1/2$, $\alpha_L > 1/2$ hosts a thermodynamic Lifshitz phase whose gap vanishes very slowly, as shown by Fig. 1.

Both the perturbative rate-equation analysis and the available numerical data point at a transition from a small- γ gapped phase to a large- γ weakly gapless Lifshitz phase when $\alpha_H < 1/2$ and $\alpha_L > 1/2$. Nevertheless, we argue that the $N \rightarrow \infty$ spectrum in this range is weakly gapless for all γ . The key observation is that the spectrum of H is bounded whereas that of L is unbounded. Hence, in the large- N limit, the largest energy scale is associated with the Lifshitz tail states of L and grows as $\sqrt{\log N}$. Consequently, as $N \rightarrow \infty$ the noise cannot be treated perturbatively. Rather, the tail states must be diagonalized out first, and only then can one apply the large- γ perturbation theory to treat their mixing with other states via H . The resulting gap dimin-

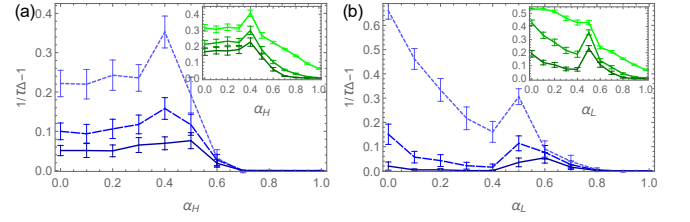


FIG. 3. (a) The relative difference between the spatial average of the relaxation rate τ^{-1} of local observables and Δ for $\gamma = 10$, $\alpha_L = 1.5$ and $N = 400$. The dotted, dashed and solid lines are based on τ^{-1} extracted by fitting the relaxation over the range $t = 3 - 6$, $6 - 9$ and $9 - 12\Delta^{-1}$, respectively. The inset shows the standard deviation of the relative difference. (b) The same quantities as a function of α_L for $\alpha_H = 1.5$.

ishes as $1/(\gamma \log N)$ but is challenging to detect: since the fixed- N , $\gamma \rightarrow 0$ perturbation theory yields a gap of order γ the tail-state eigenvector extends below it only when $N > \exp(1/\gamma^2)$. For small γ this regime is numerically inaccessible. Instead, the supplemental material demonstrates small- γ Lifshitz behavior using a model whose density of L -eigenvalues decays only as κ^{-4} .

Discussion.—Our work focused on the spectral gap Δ . To make contact with the dynamics of local observables we have followed the evolution of an initial state with $\rho_{ij} = (\delta_{ij} - \delta_{i1}\delta_{j1})/(N-1)$. We observe an asymptotic exponential approach of every ρ_{ii} to the steady state value $1/N$. The relaxation time is Δ^{-1} at all sites i , but the onset time of the asymptotic approach varies with i and depends on the overlap $(\rho_1)_{ii}$ with the slowest mode [30]. At shorter times, the relaxation is faster, due to more rapidly decaying eigenstates. These points are demonstrated by Fig. 3 and the supplemental material [30]. In terms of the natural scale Δ^{-1} the asymptotic approach begins earliest in the hydrodynamic phase, then in the gapped phase and finally in the Lifshitz phase, where most sites have only algebraically small overlap with ρ_1 .

Often, when classical noise controls the experiment, it couples to a single collective variable, e.g., the dipole moment of a chaotic quantum dot. Although we focused on this case, a more general setting involves multiple decoherence channels with their associated jump operators. In the supplemental material we extend our treatment to systems with several PRBM jump operators with exponents α_{L_k} [30]. Let us briefly quote the results. When $\tilde{\alpha}_L = \min(\alpha_{L_k}) < 1/2$, the spectrum is gapped, otherwise it is gapless. A weakly gapless Lifshitz phase occurs when $\tilde{\alpha}_L > 1/2$ and $\alpha_H < 1/2$. Finally, when all exponents exceed $1/2$ we predict a hydrodynamic regime.

Our analysis found three distinct phases as a function of the decay exponents (α_H, α_L) , but no phase transitions as a function of the decoherence strength γ . Our analysis is consistent with the possibility of transitions between gapped phases, as in Ref. [12]; indeed, we expect such transitions everywhere in the gapped phase $\alpha_L < 1/2$.

A natural question is whether the transitions we find exhibit nontrivial critical phenomena. While we have not addressed these in detail, our results shed some light on the matter. The transition from gapped to hydrodynamic relaxation as one tunes α_L at fixed $\alpha_H \gg 1$ and small γ is a transition purely in the decay rates of the hydrodynamic modes: the low-lying eigenvectors themselves evolve smoothly with α_L , and show no signs of a diverging length scale. The extended modes do change across the same transition at large γ , and further study is required. The α_H -tuned transition from Lifshitz to hydrodynamic relaxation at fixed $\alpha_L \gg 1$ appears rather simple: it is a level crossing between the localized Lifshitz tail state and the hydrodynamic mode, and as such shares some similarities with other spectral “first-order” transitions [31]. Finally, the transition between gapped and Lifshitz relaxation at $\alpha_H < 1/2$ as one tunes α_L through $1/2$ is a nontrivial critical point, associated with the emergence of tails in the density of states of PRBMs [3]. This transition is a particularly promising candidate for experimental studies in ion traps, which allow to realize power-law couplings with tunable exponents [32].

We acknowledge support by the United States-Israel Binational Science Foundation (Grant No. 2018159). The Flatiron Institute is a division of the Simons Foundation.

-
- [1] C. W. J. Beenakker, *Rev. Mod. Phys.* **69**, 731 (1997).
 - [2] L. D’Alessio, Y. Kafri, A. Polkovnikov, and M. Rigol, *Adv. Phys.* **65**, 239 (2016).
 - [3] A. D. Mirlin, Y. V. Fyodorov, F.-M. Dittes, J. Quezada, and T. H. Seligman, *Phys. Rev. E* **54**, 3221 (1996).
 - [4] M. P. A. Fisher, V. Khemani, A. Nahum, and S. Vijay, *Annu. Rev. Condens. Matter Phys.* **14**, 335 (2023).
 - [5] V. Rosenhaus, *J. Phys. A* **52**, 323001 (2019).
 - [6] R. Grobe and F. Haake, *Phys. Rev. Lett.* **62**, 2893 (1989).
 - [7] F. Haake and K. Życzkowski, *Phys. Rev. A* **42**, 1013(R) (1990).
 - [8] B. Mehlige and J. T. Chalker, *J. Math. Phys.* **41**, 3233 (2000).
 - [9] Y. V. Fyodorov and H.-J. Sommers, *J. Phys. A* **36**, 3303 (2002).
 - [10] Z. Xu, L. P. García-Pintos, A. Chenu, and A. del Campo, *Phys. Rev. Lett.* **122**, 014103 (2019).
 - [11] S. Denisov, T. Laptjeva, W. Tarnowski, D. Chruściński, and K. Życzkowski, *Phys. Rev. Lett.* **123**, 140403 (2019).
 - [12] T. Can, V. Oganessian, D. Orgad, and S. Gopalakrishnan, *Phys. Rev. Lett.* **123**, 234103 (2019).
 - [13] T. Can, *J. Phys. A* **52**, 485302 (2019).
 - [14] L. Sá, P. Ribeiro, and T. Prosen, *J. Phys. A* **53**, 305303 (2020).
 - [15] L. Sá, P. Ribeiro, and T. Prosen, *Phys. Rev. X* **10**, 021019 (2020).
 - [16] K. Wang, F. Piazza, and D. J. Luitz, *Phys. Rev. Lett.* **124**, 100604 (2020).
 - [17] S. Lange and C. Timm, *Chaos* **31**, 023101 (2021).
 - [18] W. Tarnowski, T. Yusipov, I. Laptjeva, S. Denisov, D. Chruściński, and K. Życzkowski, *Phys. Rev. E* **104**, 034118 (2021).
 - [19] V. Popkov and C. Presilla, *Phys. Rev. Lett.* **126**, 190402 (2021).
 - [20] J. L. Li, D. C. Rose, J. P. Garrahan, and D. J. Luitz, *Phys. Rev. B* **105**, L180201 (2022).
 - [21] L. Sá, P. Ribeiro, and T. Prosen, *Phys. Rev. Research* **4**, L022068 (2022).
 - [22] A. Kulkarni, T. Numasawa, and S. Ryu, *Phys. Rev. B* **106**, 075138 (2022).
 - [23] A. D. Mirlin and F. Evers, *Phys. Rev. B* **62**, 7920 (2000).
 - [24] I. Varga and D. Braun, *Phys. Rev. B* **61**, R11859 (2000).
 - [25] O. Yevtushenko and V. E. Kravtsov, *Phys. Rev. E* **69**, 026104 (2004).
 - [26] We draw the matrices representing H and L in an uncorrelated way. Hence, they do not commute with probability 1. In case they commute, the Lindbladian \mathcal{L} possesses N steady states given by the populations $|i\rangle\langle i|$, where $|i\rangle$ are the simultaneous eigenstates of H and L .
 - [27] S. Yao and Z. Wang, *Phys. Rev. Lett.* **121**, 086803 (2018).
 - [28] J. Bensa and M. Žnidarič, *Phys. Rev. X* **11**, 031019 (2021).
 - [29] T. Mori and T. Shirai, *Phys. Rev. Lett.* **130**, 230404 (2023), and references therein.
 - [30] See Supplemental Material for additional details on the properties of PRBMs. We also include numerical data on the behavior of the populations rate equations at weak and strong decoherence alongside an analytical treatment of their mean-field approximation. The supplemental material also contains results for a related model that exhibits a Lifshitz phase at weak decoherence, systems with multiple jump operators, and the dynamics of local observables.
 - [31] M. M. Parish, *Phys. Rev. A* **83**, 051603 (2011).
 - [32] P. Richerme, Z.-X. Gong, A. Lee, C. Senko, J. Smith, M. Foss-Feig, S. Michalakakis, A. V. Gorshkov, and C. Monroe, *Nature* **511**, 198 (2014).

Supplemental Material for: "Dynamical transition from slow to fast relaxation in random open quantum systems"

Dror Orgad¹, Vadim Oganesyan^{2,3}, and Sarang Gopalakrishnan⁴

¹*Racah Institute of Physics, The Hebrew University, Jerusalem 91904, Israel*

²*Department of Physics and Astronomy, College of Staten Island, CUNY, Staten Island, NY 10314, USA*

³*Center for Computational Quantum Physics, Flatiron Institute, 162 5th Avenue, New York, NY 10010, USA*

⁴*Department of Electrical and Computer Engineering, Princeton University, Princeton, NJ 08540, USA*

CONTENTS

I. Power-Law Random Banded Matrices	1
II. Effective dynamics of populations	3
A. Effective dynamics in the limits of weak and strong decoherence	3
B. Slowest decaying mode of A for $\gamma \rightarrow 0, \infty$	4
C. Finite size scaling of $\Delta(A)$	5
D. Comparing \mathcal{L} and A	6
E. Small γ and $\alpha_H > 1$	10
F. Small γ and $\alpha_H < 1/2$	13
1. $N < \exp(4/\gamma^2)$	13
2. $N > \exp(4/\gamma^2)$	14
G. Small γ and $1 > \alpha_H > 1/2$	16
H. Large γ and $\alpha_L < 1/2$	17
I. Large γ and $1 > \alpha_L > 1/2$	18
J. Large γ and $\alpha_L > 1$	19
III. Multiple jump operators	20
IV. Dynamics of local observables	25

I. POWER-LAW RANDOM BANDED MATRICES

Consider an $N \times N$ random matrix, G , belonging to one of the Gaussian ensembles. From it, one can derive a power-law random banded matrix (PRBM), H , whose elements are defined by

$$H_{ij} = f_{ij} G_{ij}, \quad f_{ij} = f_{|i-j|} = \frac{1}{\delta_{ij} + |i-j|^\alpha}. \quad (1)$$

We dub the basis for which Eq. (1) holds the x -basis. For a system with periodic boundary conditions the appropriate variant is the circulant power-law random banded matrix (CPRBM), for which

$$f_{ij} = \frac{1}{\delta_{ij} + (N/2 - |N/2 - |i-j||)^\alpha}. \quad (2)$$

Varying the exponent α changes the scaling of the spread of the spectrum with N . In order to avoid this effect we consider in the following PRBM (and CPRBM) ensembles which are derived from matrices G drawn from the GOE

$$P(G) \propto \exp \left[-\frac{a(N, \alpha)}{2} \text{Tr} (G^2) \right], \quad (3)$$

with

$$a(N, \alpha) = 1 + \sum_{j=1}^{N-1} f_{N/2,j}^2 = 2 + 2h\left(\frac{N}{2} - 1, 2\alpha\right) \xrightarrow{N \rightarrow \infty} 2 + 2\left[\frac{(N/2)^{1-2\alpha}}{1-2\alpha} + \zeta(2\alpha)\right]. \quad (4)$$

Here $h(N, \alpha) = \sum_{n=1}^N n^{-\alpha}$ is the harmonic number of order α and $\zeta(\alpha)$ is the zeta function. Consequently,

$$\langle H_{ij} H_{kl} \rangle = \frac{f_{ij}^2}{2a(N, \alpha)} (\delta_{ik} \delta_{jl} + \delta_{il} \delta_{jk}), \quad (5)$$

thus implying that the variance of the sum of elements in a (middle) row of H is $1/2$ (up to $1/N$ corrections), irrespective of α . This in turn leads to a spectrum whose standard deviation is $1/\sqrt{2}$.

The spectral properties of the GOE-derived PRBM ensemble were studied by Mirlin *et al.* using a non-linear sigma model (NLSM).[1] For $\alpha < 1/2$ all statistical properties are predicted to coincide with those of the GOE. In particular, the density of states (DOS) is given by Wigner's semicircle law and the eigenstates, v , are delocalized, as revealed by the behavior of their inverse participation ratio (IPR) $I = \sum_{i=1}^N |v_i|^4$, whose mean scales as $\langle I \rangle \propto 1/N$ and whose relative variance follows $\delta(I) = (\langle I^2 \rangle - \langle I \rangle^2) / \langle I \rangle^2 \propto 1/N$. Such behavior is confirmed numerically, see Figs. 1, 2.

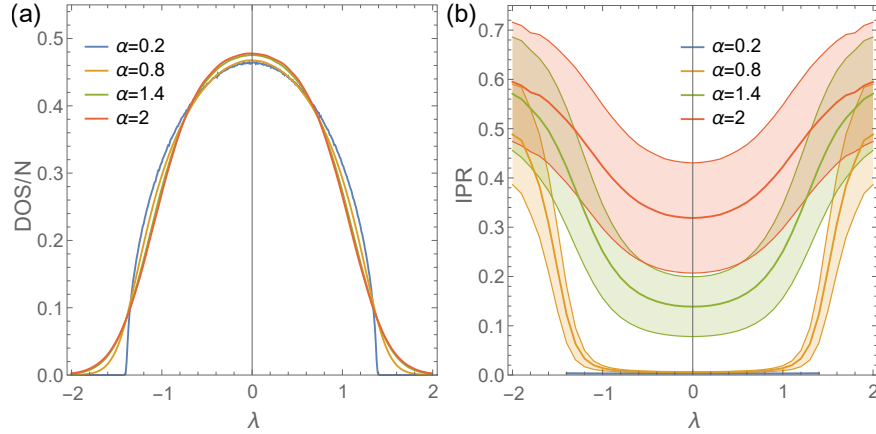


FIG. 1. (a) PRBM eigenvalue distribution for various exponents α . We use a normalization that keeps the spectrum variance at $1/2$ for all α . Gaussian tails appear for $\alpha > 1/2$. (b) The average IPR of the eigenstates. The bands half width corresponds to the IPR standard deviation. Localization transition occurs at $\alpha = 1$ but localized tail states exist for $\alpha > 1/2$.

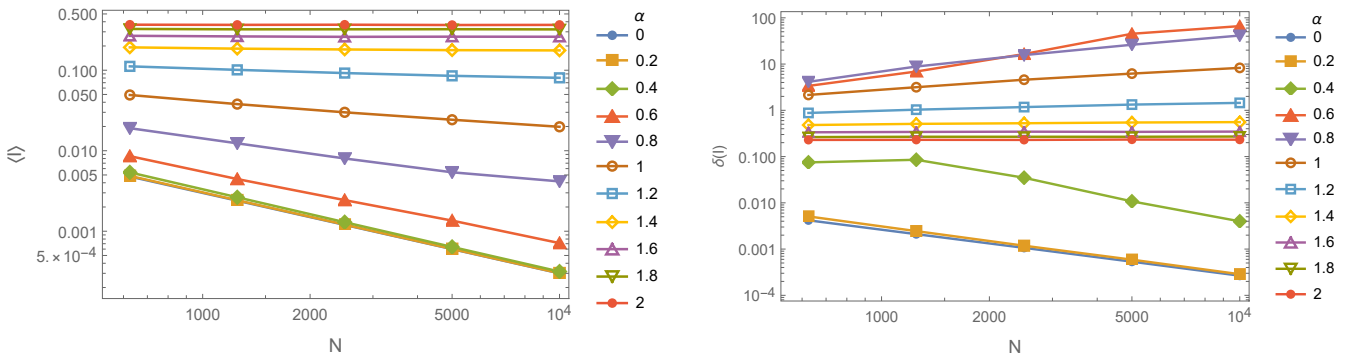


FIG. 2. N -dependence of the average inverse participation ratio and its relative variance. For $\alpha < 1/2$ both quantities scale as $1/N$. The results shown are for CPRBM but change little for PRBM.

On the other hand, for $\alpha > 1/2$ the DOS deviates from the semicircle and develops Gaussian tails [2] (we observe similar tails also when the entries of G are box-distributed instead of normal). In the range $1 > \alpha > 1/2$ the mean IPR continues to decay with N . However, it does so more slowly than $1/N$, which is the NLSM prediction for $\alpha < 1$.

The IPR fluctuations in this range are also stronger than the NLSM predictions, and numerically we find that $\delta(I)$ increases in the available range of N . We attribute this behaviour to the appearance of localized states at the tails of the spectrum, as depicted in Fig. 1. These states decay algebraically $|\psi(x)| \sim |x|^{-\alpha}$ and their number, n_{loc} , increases in a sublinear manner with N . Results of fitting n_{loc} to a power law in N together with a typical decay of a localized state are shown in Fig. 3. Finally, for $\alpha > 1$, $O(N)$ eigenstates are power-law ($|x|^{-\alpha}$) localized leading to $\langle I \rangle > 0$.

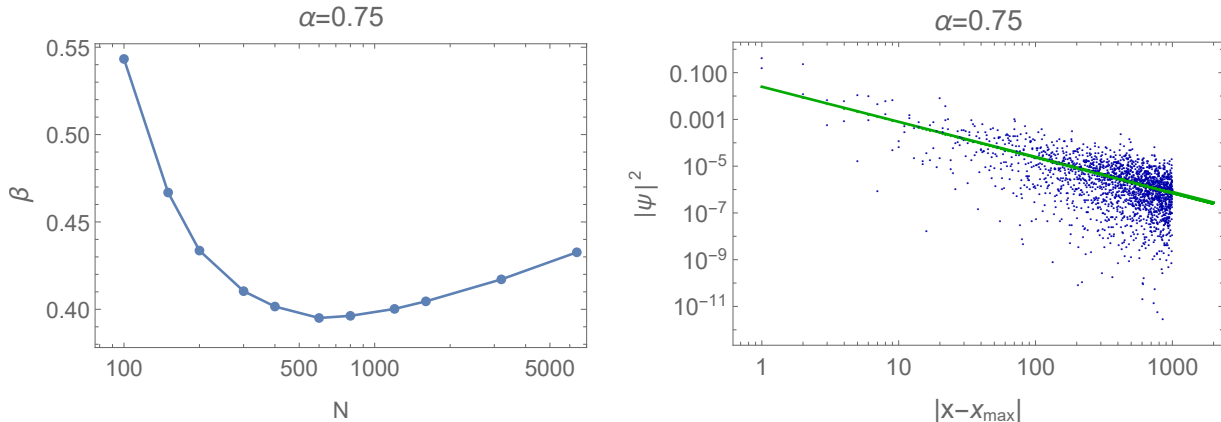


FIG. 3. Left: Fitting n_{loc} , defined as the average number of states with $\text{IPR} > 0.1$, to a power law $n_{\text{loc}} = N^\beta$. Right: The decay of a localized tail state as a function of the distance from its peak. The solid line depicts a $|x - x_{\text{max}}|^{-1.5}$ decay.

II. EFFECTIVE DYNAMICS OF POPULATIONS

A. Effective dynamics in the limits of weak and strong decoherence

In the limits of vanishing and infinitely strong decoherence the Lindbladian spectrum contains N zero modes given by the populations of Hamiltonian eigenstates (H -populations) and of L -eigenstates (L -populations), respectively. This degeneracy is lifted away from the strict $\gamma = 0, \infty$ limits with only the infinite temperature thermal state $\rho_{ss} = \mathbb{1}/N$ remaining as a steady state for arbitrary γ . Nevertheless, one expects that at weak decoherence the slowest decaying mode consists primarily of H -populations, while for strong decoherence it is largely composed of L -populations. This expectation is confirmed numerically, as shown by Fig. 2 of the main text and by supplemental Fig. 4. The figures also show that the strongest mixing of coherences into the state occurs for $\alpha_H < 1$ at weak decoherence and for $\alpha_H > 1/2$ and $1 > \alpha_L > 1/2$ at strong decoherence. The mixing increases with N .

More specifically, by considering the limits $\gamma \rightarrow 0, \infty$ for fixed N one may obtain an asymptotically exact description of the low-lying \mathcal{L} -eigenstates in terms of the populations alone [3]. We begin by considering weak decoherence and express \mathcal{L} in the eigenbasis of H , where $H_{ij} = \epsilon_i \delta_{ij}$. For the case of interest, where H and L are real and symmetric, the effective description is given by [3]

$$A_{ij} = -\gamma [L_{ij}^2 \delta_{ij} - (L_{ij})^2]. \quad (6)$$

Conversely, in the limit of strong decoherence we express \mathcal{L} in the eigenbasis of L , where $L_{ij} = \kappa_i \delta_{ij}$. The effective description within the population subspace is governed by the matrix [3]

$$\begin{aligned} A_{ij} &= \frac{4}{\gamma} \frac{H_{ij}^2 (\kappa_i - \kappa_j)^2}{(\kappa_i - \kappa_j)^4 + (2/\gamma)^2 (H_{ii} - H_{jj})^2} \quad \text{for } i \neq j, \\ A_{ii} &= -\sum_{j \neq i} A_{ij}. \end{aligned} \quad (7)$$

Physically, Eq. (7) describes Hamiltonian-induced hopping between L -population via L -coherences. Despite being higher order in $1/\gamma$ we have kept (in the second term of the denominator) the H -induced shift in the eigenvalues of the coherences. As we show below, it may induce delocalization of the slowest decaying mode in the large α_H, α_L regime when γ is fixed and $N \rightarrow \infty$.

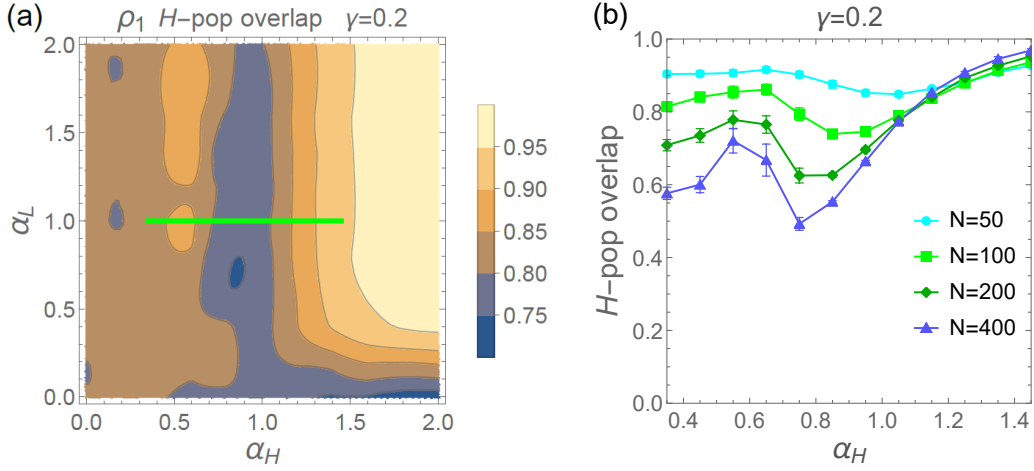


FIG. 4. (a) The average overlap (the norm of the projected vector) between the slowest decaying mode ρ_1 and the subspace of H -populations at weak decoherence $\gamma = 0.2$ and $N = 100$. (b) N -dependence of the overlap along the cut shown in (a).

B. Slowest decaying mode of A for $\gamma \rightarrow 0, \infty$

Here we present data obtained by diagonalizing A in the limits $\gamma \rightarrow 0, \infty$ for the largest systems that we considered. The left panel of Fig. 5 shows the spectral gap for vanishing γ while the other two panels concern the corresponding slowest decaying mode and depict its inverse participation ratio in energy space, IPR_H , and in position space, IPR_X . The latter are defined via the expansion of the mode in the energy basis $\rho^{(1)} = \sum_{i=1}^N \rho_i |i\rangle \langle i|$ as

$$\text{IPR}_H = \sum_{i=1}^N \rho_i^4, \quad (8)$$

$$\text{IPR}_X = \sum_{i=1}^N \rho_i^4 \sum_{x=1}^N |\langle x|i\rangle|^4, \quad (9)$$

where $|x\rangle$ is the x -basis.

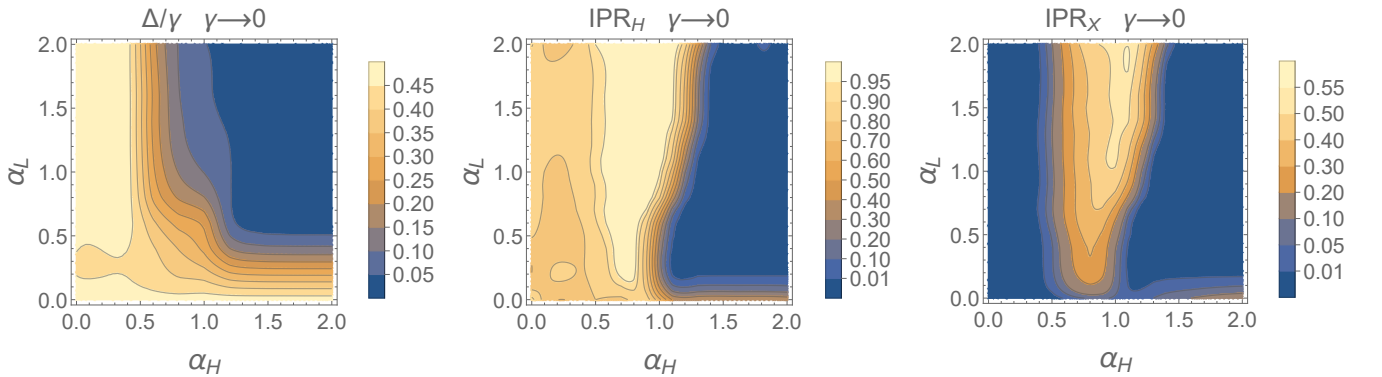


FIG. 5. Left: The spectral gap of A in the limit of vanishing decoherence for an $N = 12800$ system whose Hamiltonian and jump operator are PRBMs with exponents α_H and α_L , respectively. Center and right: The inverse participation ratios in energy space and in real space of the corresponding slowest decaying mode for a system with $N = 6400$. The data was averaged over 100 realizations for each (α_H, α_L) point.

Fig. 6 shows similar data obtained by diagonalizing Eq. (7) in the limit $\gamma \rightarrow \infty$. For this case we expand the slowest decaying mode in the L -populations and use the expansion coefficients to define the inverse participation ratio in the L -eigenbasis, IPR_L , and in the position basis using Eqs. (8,9).

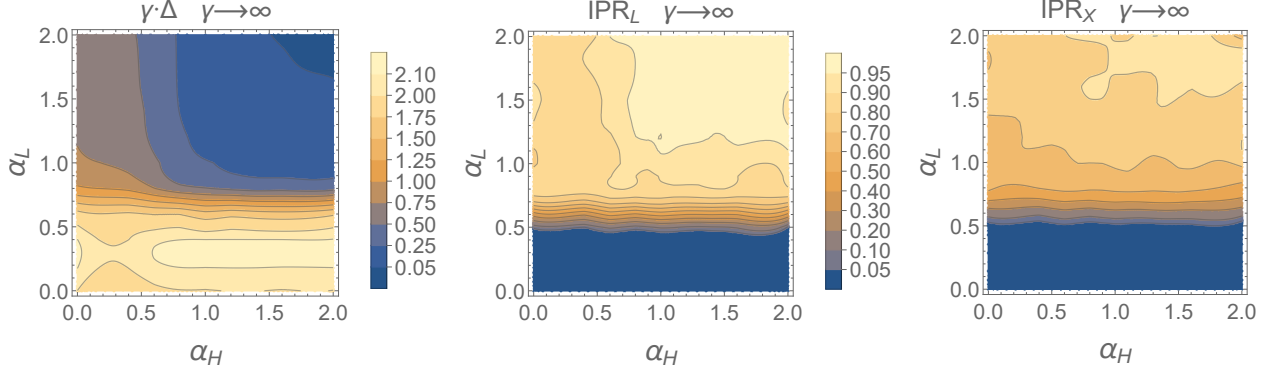


FIG. 6. Left: The spectral gap of A in the limit of $\gamma \rightarrow \infty$ for an $N = 12800$ system whose Hamiltonian and jump operator are PRBMs with exponents α_H and α_L , respectively. Center and right: The inverse participation ratios in the L -basis and in real space of the corresponding slowest decaying mode for a system with $N = 6400$. We note that an additional region of extended states exists outside the depicted parameters range for $\alpha_L > 3$ and $\alpha_H > 3/2$, see bottom row of Fig. 8.

C. Finite size scaling of $\Delta(A)$

Figs. 7 and 8 contain the finite size scaling of the spectral gap calculated from A for system sizes of up to $N = 12800$. The results were obtained using Eq. (6) and Eq. (7) corresponding to the limits $\gamma \rightarrow 0$ and $\gamma \rightarrow \infty$, respectively. Each point represents an average over 100-300 realizations.

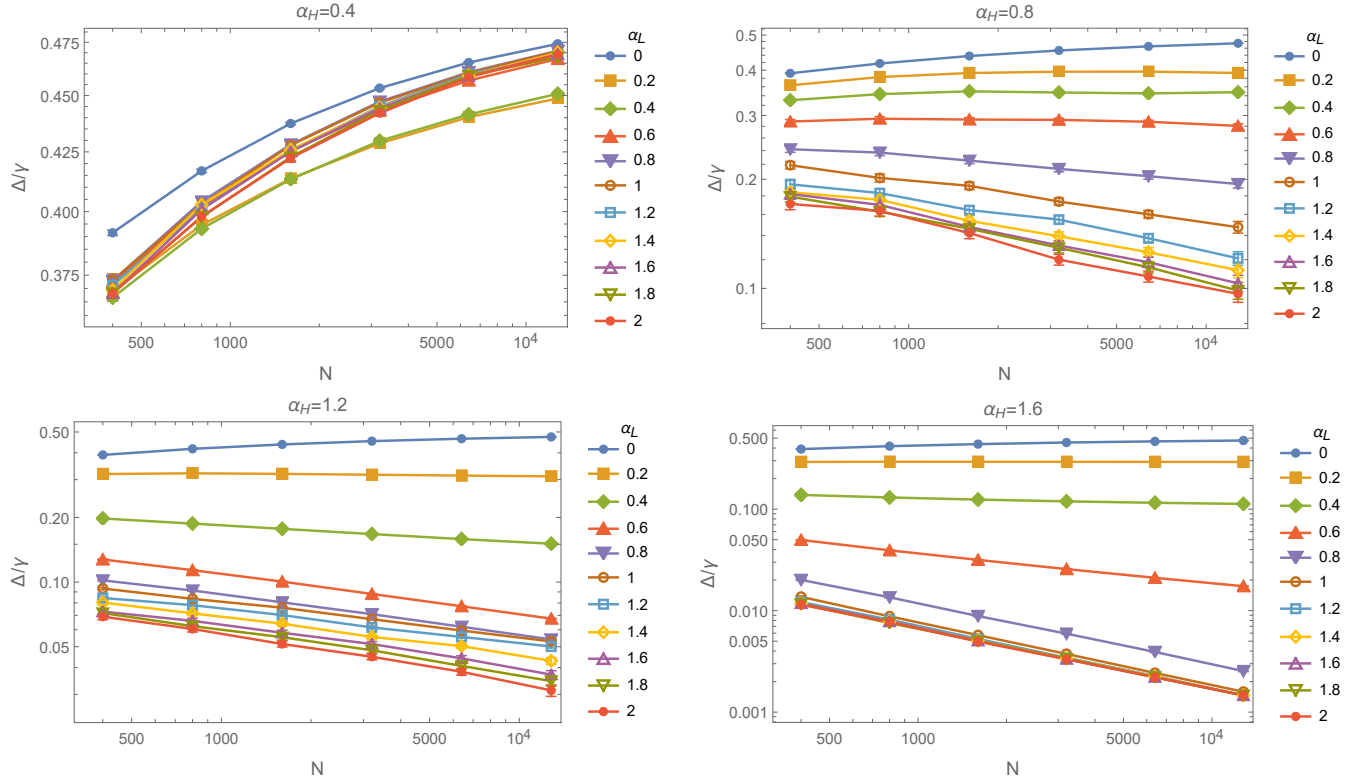


FIG. 7. N -dependence of the gap calculated from A in the limit $\gamma \rightarrow 0$.

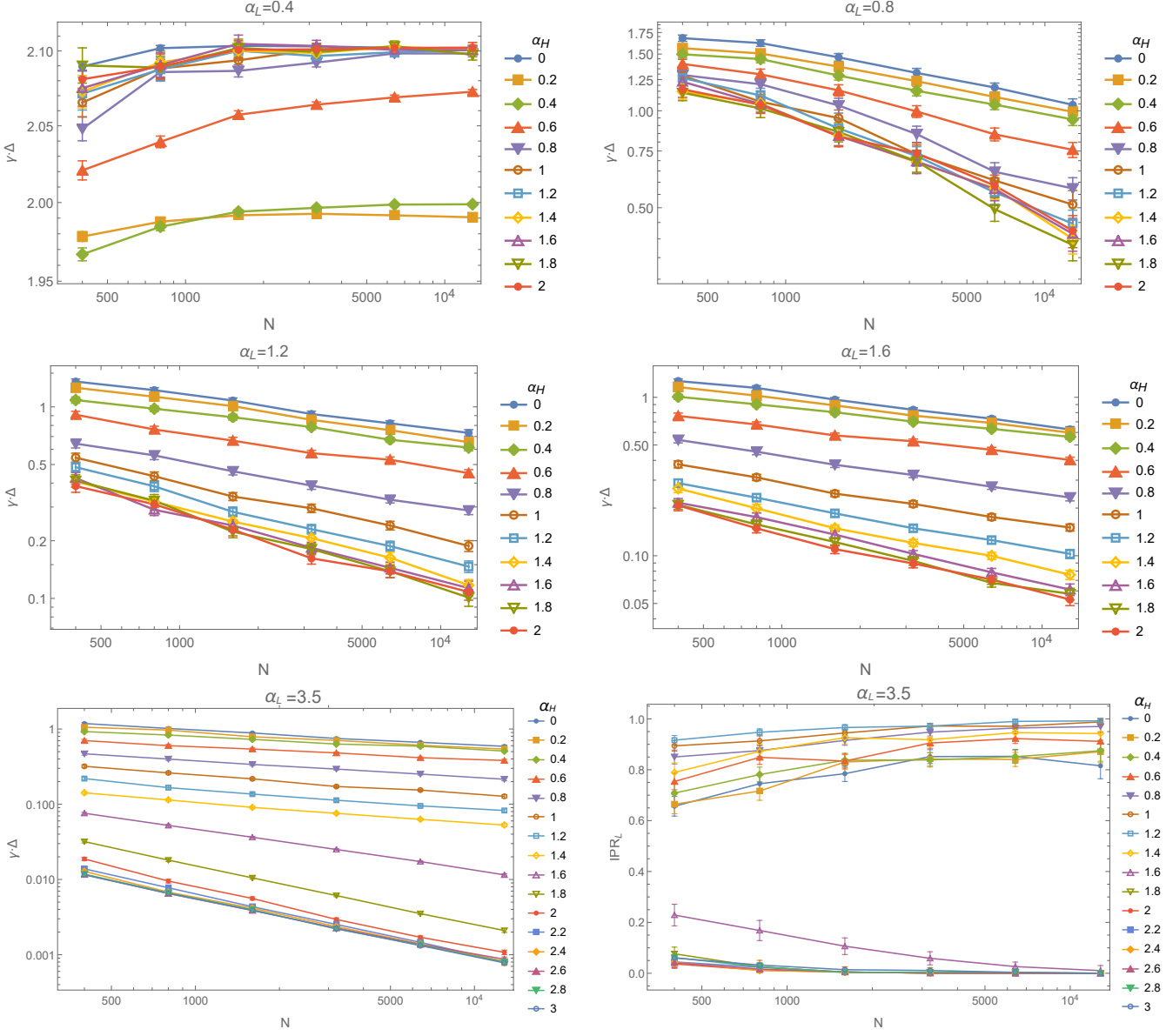


FIG. 8. N -dependence of the gap calculated from A in the limit $\gamma \rightarrow \infty$. The bottom right panel demonstrates that the slowest decaying mode in this limit becomes extended for $\alpha_L > 3$ and $\alpha_H > 3/2$. Concomitantly, the gap decays more rapidly with N .

D. Comparing \mathcal{L} and A

The effective populations dynamics generated by Eqs. (6,7) provides an asymptotically exact description of the low-lying Lindbladian states for fixed N and $\gamma \rightarrow 0, \infty$. However, we would like to assess its validity away from the extreme γ limits, and in particular when $N \rightarrow \infty$ while γ is held fixed. To this end, we have calculated the properties of the slowest decaying Lindbladian mode, averaged over 100 realizations per (α_H, α_L) point, and compared them with the corresponding results obtained by diagonalizing A , given by Eqs. (6) and (7). Fig. 9 shows that the general dependence of the spectral gap on α_H and α_L is captured reasonably well by A , at least for the system sizes amenable to exact diagonalization of \mathcal{L} . However, qualitative deviations are expected at weak decoherence for $\alpha_H < 1/2$ in the very large N limit, see Sec. II F. We also note that the relative error between the gap calculated from A and the one calculated from \mathcal{L} , $[\Delta(A) - \Delta(\mathcal{L})]/\Delta(\mathcal{L})$, increases with N , as shown by Fig. 10. Nevertheless, note that we always find $\Delta(A) > \Delta(\mathcal{L})$, thus strongly suggesting an upper bound on the exact gap, and convergence of the two gaps in the extreme γ limits for fixed N .

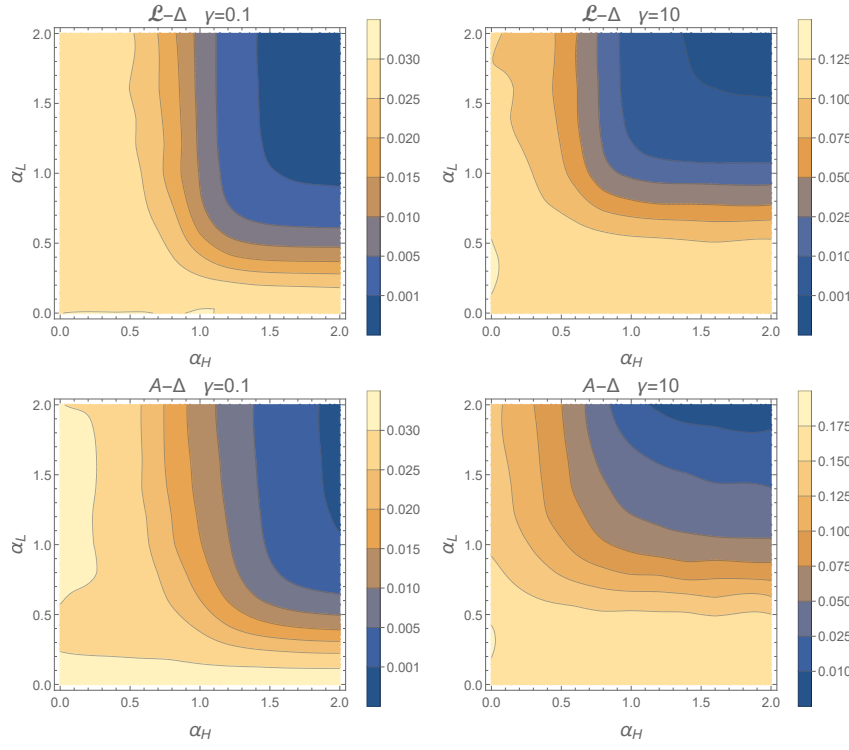


FIG. 9. Left: The spectral gap as calculated from the full Lindbladian and from the effective population dynamics, Eq.(6) for $\gamma = 0.1$ and Eq. (7) for $\gamma = 10$, of a system with $N = 100$.

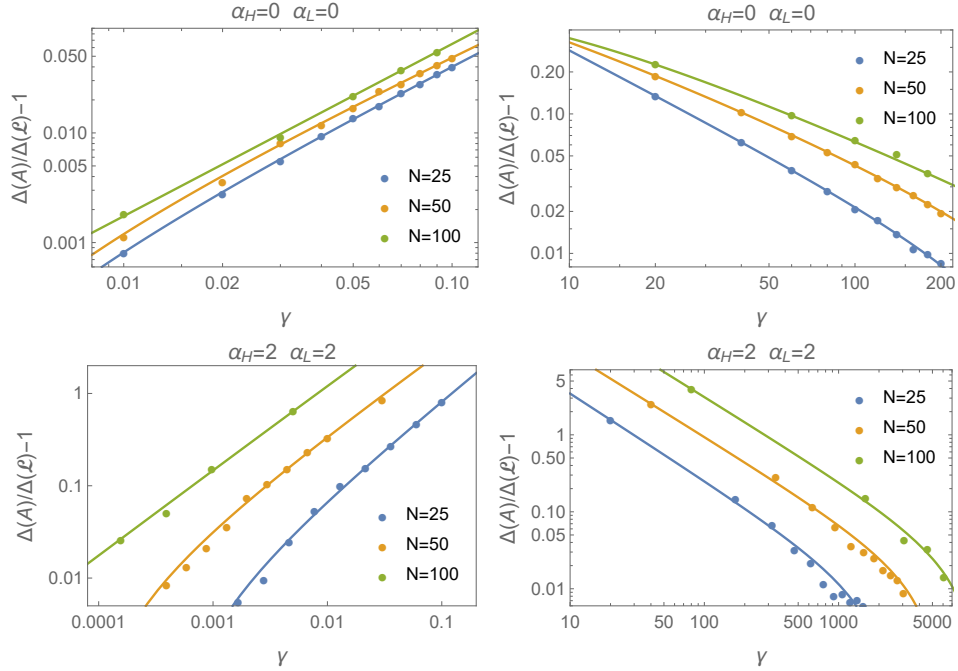


FIG. 10. Left: The relative error between the gap calculated from A and the exact gap calculated from \mathcal{L} for weak and strong decoherence. Results are shown for systems with $N = 25, 50$ and 100 in the cases where both H and L are GOE random matrices ($\alpha_H = \alpha_L = 0$) and where they are both PRBMs in the localized regime ($\alpha_H = \alpha_L = 2$). The lines are guides to the eye.

We have also calculated the inverse participation ratio of the slowest decaying Lindbladian mode projected on the H -populations space (IPR_H) and on the L -populations space (IPR_L). Concretely, if the expansion of the mode in

the energy basis reads $\rho^{(1)} = \sum_{i,j} \rho_{ij} |i\rangle\langle j|$, with $\sum_{i,j} |\rho_{ij}|^2 = 1$ then

$$\text{IPR}_H = \frac{\sum_i \rho_{ii}^4}{(\sum_i \rho_{ii}^2)^2}. \quad (10)$$

IPR_L is defined in a similar manner using the expansion of ρ in the L basis. In addition, we calculated the real space IPR of the mode, which for small γ we define using the above energy basis expansion of ρ as

$$\text{IPR}_X = \frac{\sum_i \rho_{ii}^4 \sum_x |\langle x|i \rangle|^4}{(\sum_i \rho_{ii}^2)^2}. \quad (11)$$

This quantifier approaches 1 if the projected mode is largely composed of a single population of a real-space localized energy eigenstate, and else vanishes in the thermodynamic limit. For large γ we define IPR_x in a similar fashion using the L -basis expansion of $\rho^{(1)}$.

Figs. 11,12 show that the population dynamics broadly captures the nature of the slowest mode within the α_H - α_L plane, albeit with a tendency to overestimate the range in which it is localized. This is particularly true for $\gamma = 10$ where the decrease of the IPR is recovered only at $\alpha_L > 3/2$. We note that for this to happen one must include the eigenvalue shifts in Eq. (7). Without it, the A -IPR is large for all $3 > \alpha_L > 1/2$. The figures also show that for small γ the \mathcal{L} -slowest mode becomes delocalized both in energy and real space. As shown in the main text, for large γ this mode remains localized in the region $\alpha_H < 1/2$, $\alpha_L > 1/2$.

Finally, we have compared the averaged populations density of states (P-DOS). For \mathcal{L} the latter was obtained by picking among the eigenstates with real eigenvalues the N (there are at least as many for the case of an Hermitian L [3]) whose overlaps with the H -populations (for small γ) or L -populations (large γ) are the largest. Fig. 13 shows that A essentially reproduces the exact DOS in the case of weak decoherence. For strong decoherence it overestimates the width of the P-DOS, as seen in Fig. 14. We note that this overestimation is made much worst if one does not include the spectral shifts in the denominator of Eq. (7).

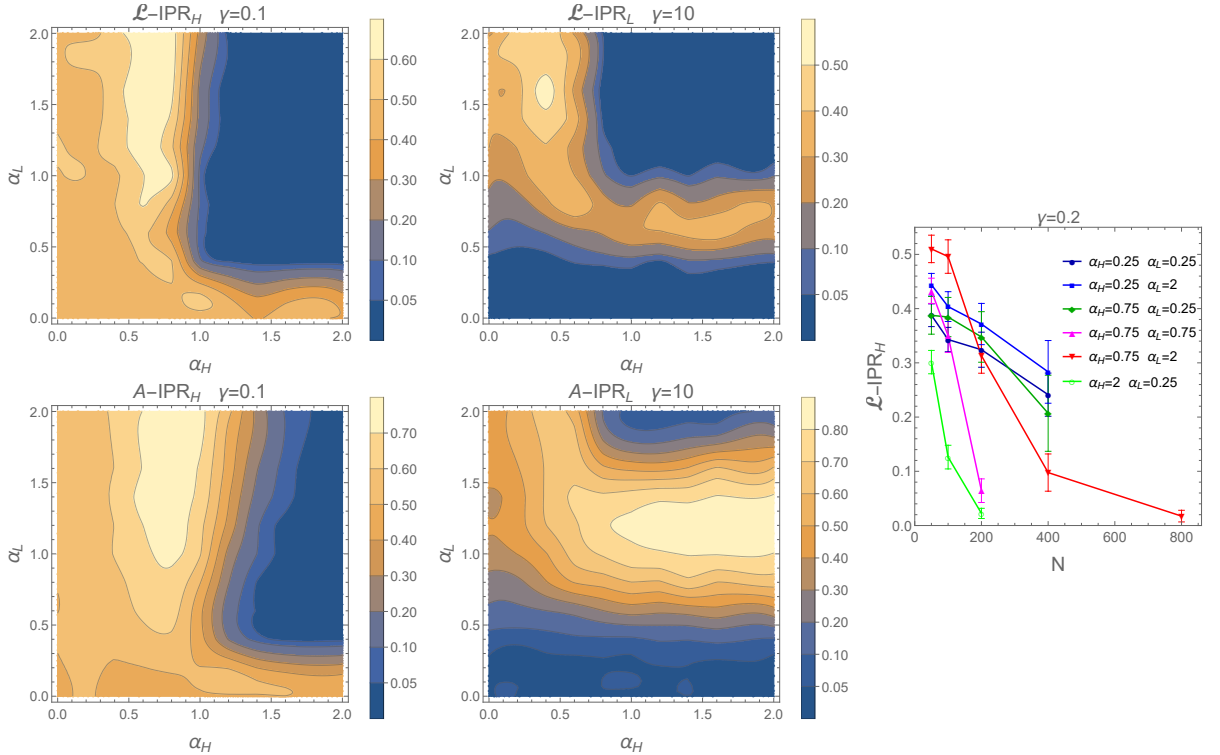


FIG. 11. Left: The average inverse participation ratio in energy space of the slowest decaying mode as calculated from \mathcal{L} and A for a system with $\gamma = 0.1$, $N = 100$. Middle: The average participation ratio in the space of L -eigenvectors of the slowest decaying mode for $\gamma = 10$ and $N = 100$. Right: System size dependence of the IPR_H of the slowest decaying \mathcal{L} -mode for a system with $\gamma = 0.2$.

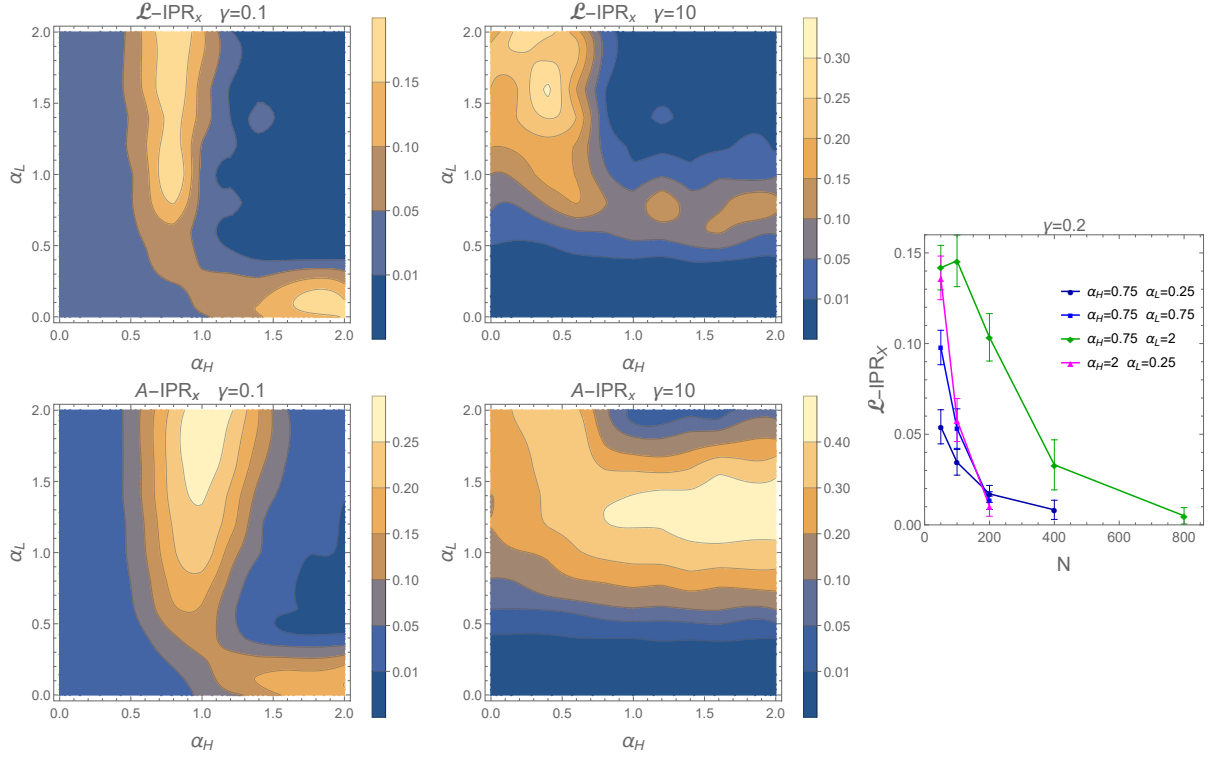


FIG. 12. Left: The average inverse participation ratio in real space of the slowest decaying mode as calculated from \mathcal{L} and A for an $N = 100$ system. Right: System size dependence of the IPR_x of the slowest decaying \mathcal{L} -mode for a system with $\gamma = 0.2$.

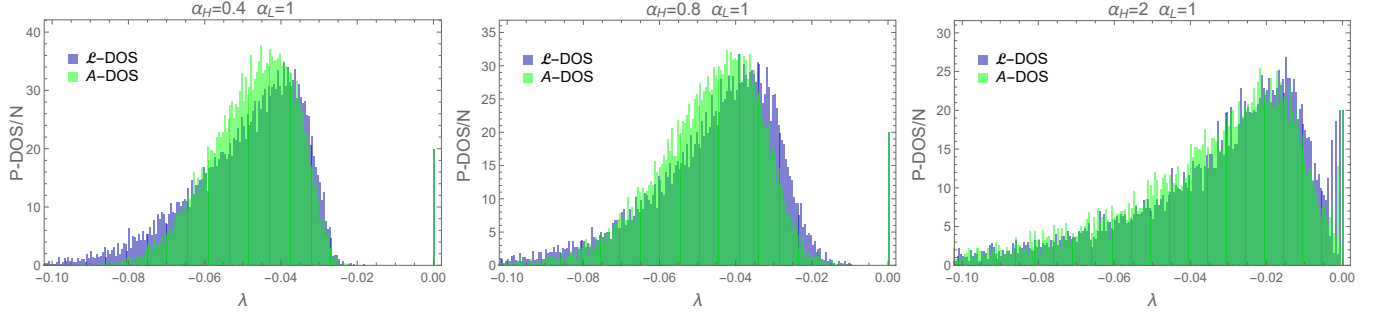


FIG. 13. The averaged population DOS calculated from \mathcal{L} and A for a system with $\gamma = 0.1$, $N = 100$ and representative values of (α_H, α_L) .

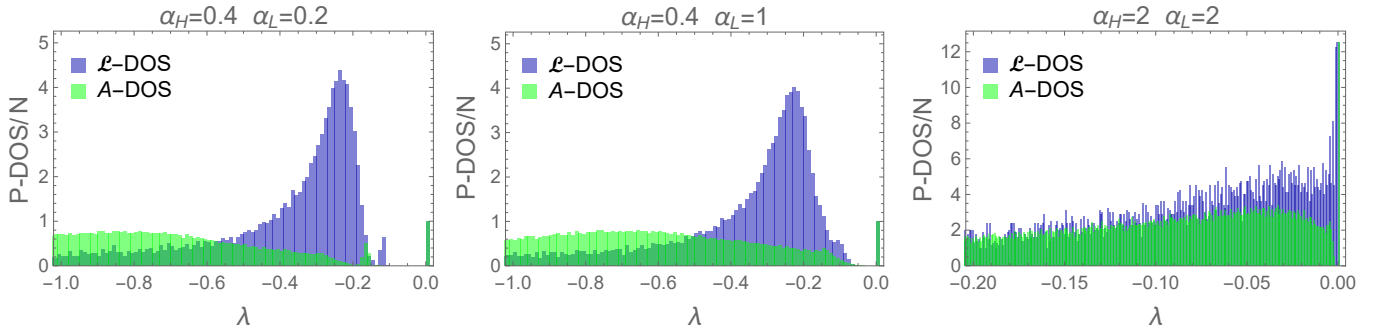


FIG. 14. The averaged populations DOS calculated from \mathcal{L} and A for a system with $\gamma = 10$, $N = 100$ and representative values of (α_H, α_L) .

E. Small γ and $\alpha_H > 1$

Denote by L_0 the PRBM describing the jump operator in the x -basis and by U the unitary that diagonalizes the Hamiltonian: $H = U^\dagger \varepsilon U$, with ε a diagonal matrix containing the energy eigenvalues. Hence, $L = UL_0U^\dagger$ and Eq. (6) becomes

$$A_{ij} = -\gamma \sum_{mn} U_{im}(L_0^2)_{mn} U_{nj}^\dagger \delta_{ij} + \gamma \left| \sum_{mn} U_{im}(L_0)_{mn} U_{nj}^\dagger \right|^2. \quad (12)$$

Consider the extreme case where the eigenstates of H are localized on single sites. We expect that this limit is relevant for $\alpha_H \gg 1$. For such a model $U_{ij} = \delta_{j,P_i}$, where $P_i = P(i)$, with P some permutation of $\{1, \dots, N\}$. Consequently,

$$A_{ij} = -\gamma \left[(L_0^2)_{P_i P_j} \delta_{ij} - |(L_0)_{P_i P_j}|^2 \right] = -\gamma \sum_{mn} U_{im} \left[(L_0^2)_{mn} \delta_{mn} - |(L_0)_{mn}|^2 \right] U_{nj}^\dagger \equiv (UA_0U^\dagger)_{ij}, \quad (13)$$

and the spectrum of A coincides with that of A_0 .

Using Eq. 5 we can decompose $A_0 = \bar{A}_0 + \delta A_0$, where the elements of the constant "mean-field" part are give by

$$(\bar{A}_0)_{ij} = \langle (A_0)_{ij} \rangle_L = \frac{\gamma}{2a(N, \alpha_L)} \begin{cases} -\sum_{m \neq i} f_{L,im}^2 & i = j \\ f_{L,ij}^2 & i \neq j \end{cases}, \quad (14)$$

where $\langle \rangle_L$ denotes the mean with respect to the statistics of L_0 , and f_L is the power-law form factor associated with L . The elements of the fluctuating part are random variables with zero mean. They are not independent. Clearly, $(\delta A_0)_{ij} = (\delta A_0)_{ji}$ and $(\delta A_0)_{ii}$ contains $(\delta A_0)_{ij}$, which also means that it is not independent of $(\delta A_0)_{jj}$. Thus

$$\langle (\delta A_0)_{ij} (\delta A_0)_{ji} \rangle_L = (-1)^{1-\delta_{ij}} \langle (\delta A_0)_{ii} (\delta A_0)_{ij} \rangle_L = \langle (\delta A_0)_{ii} (\delta A_0)_{jj} \rangle_L = \frac{\gamma^2}{2a^2(N, \alpha_L)} \begin{cases} \sum_{m \neq i} f_{L,im}^4 & i = j \\ f_{L,ij}^4 & i \neq j \end{cases}. \quad (15)$$

For a CPRBM jump operator the eigenvalues of \bar{A}_0 are given by (we assume here odd N)

$$\lambda_n = -\frac{2\gamma}{a(N, \alpha_L)} \sum_{j=1}^{(N-1)/2} f_{L,j}^2 \sin^2 \left(\frac{j\pi n}{N} \right). \quad n = 0, \dots, \frac{N-1}{2}, \quad (16)$$

and apart from the zero mode $(v_0)_j = 1/N$, every eigenvalue is doubly degenerate with the corresponding (normalized) eigenvectors

$$(v_n)_j = \sqrt{\frac{2}{N}} \cos \left(\frac{2\pi n j}{N} \right), \quad (u_n)_j = \sqrt{\frac{2}{N}} \sin \left(\frac{2\pi n j}{N} \right), \quad n = 1, \dots, \frac{N-1}{2}. \quad (17)$$

In order to evaluate the spectral gap we require the large- N behavior of

$$\begin{aligned} \sum_{j=1}^{(N-1)/2} f_j^2 \sin^2 \left(\frac{j\pi}{N} \right) &\xrightarrow{N \rightarrow \infty} N^{1-2\alpha} \int_{1/N}^{1/2} dx x^{-2\alpha} \sin^2(\pi x) \\ &\xrightarrow{N \rightarrow \infty} \frac{(N/2)^{1-2\alpha}}{2(1-2\alpha)} \left[1 - {}_1F_2 \left(\frac{1}{2} - \alpha, \left\{ \frac{1}{2}, \frac{3}{2} - \alpha \right\}, -\frac{\pi^2}{4} \right) \right] - \frac{\pi^2}{3-2\alpha} \frac{1}{N^2}, \end{aligned} \quad (18)$$

where ${}_1F_2$ is the generalized hypergeometric function and which leads, together with Eq. (4), to the gap

$$\Delta = \begin{cases} -\frac{\gamma}{2} \left[1 - {}_1F_2 \left(\frac{1}{2} - \alpha_L, \left\{ \frac{1}{2}, \frac{3}{2} - \alpha_L \right\}, -\frac{\pi^2}{4} \right) \right] \left[1 - (1-2\alpha_L)[1 + \zeta(2\alpha_L)] \left(\frac{2}{N} \right)^{1-2\alpha_L} \right] & \alpha_L < 1/2 \\ -\frac{\gamma}{2(1-2\alpha_L)[1+\zeta(2\alpha_L)]} \left[1 - {}_1F_2 \left(\frac{1}{2} - \alpha_L, \left\{ \frac{1}{2}, \frac{3}{2} - \alpha_L \right\} \right) \left(\frac{2}{N} \right)^{2\alpha_L-1} \right] & 3/2 > \alpha_L > 1/2 \\ -\frac{\gamma\pi^2}{(2\alpha_L-3)[1+\zeta(2\alpha_L)]} \frac{1}{N^2} & \alpha_L > 3/2 \end{cases}. \quad (19)$$

Consider now the effects of δA_0 on the gap. The zero-mode is guaranteed and to lowest order we need to diagonalize δA_0 within the degenerate subspace spanned by v_1 and u_1 (note that for $\alpha_L = 0$ the \bar{A}_0 spectrum is $(N - 1)$ -fold degenerate at $-\gamma/2$). To this end we note that $\langle\langle u|\delta A_0|v\rangle\rangle_L = 0$ and use Eq. (15) to obtain

$$\begin{aligned} \sqrt{\langle\langle u|\delta A_0|v\rangle\rangle_L^2} &= \left\{ \left\langle \left(\sum_{i \neq j} u_i v_j (\delta A_0)_{ij} + \sum_i u_i v_i (\delta A_0)_{ii} \right) \left(\sum_{k \neq l} u_k v_l (\delta A_0)_{kl} + \sum_k u_k v_k (\delta A_0)_{kk} \right) \right\rangle_L \right\}^{1/2} \\ &= \frac{\gamma}{\sqrt{2}a(N, \alpha_L)} \left[\sum_{i \neq j} [u_i^2(v_i^2 + v_j^2) + 2u_i u_j v_i v_j - 2u_i^2 v_i v_j - 2u_i u_j v_j^2] f_{L,ij}^4 \right]^{1/2}, \end{aligned} \quad (20)$$

which scales as $1/N$ and $1/\sqrt{N}$ in the limits $\alpha_L \rightarrow 0$ and $\alpha_L \rightarrow \infty$, respectively. Together with Eq. (19) this signals the breakdown of perturbation theory for large α_L . Since the difference $\lambda_1 - \lambda_2$ scales to a constant as $\alpha_L \rightarrow 0$ we expect that in this limit the effects of the fluctuating part diminish for $N \rightarrow \infty$.

The above analysis is backed by our numerics. As demonstrated by Fig. 15, the gap largely follows Eq. (16) with deviations at small α_L that diminish upon increasing N . An important lesson from the numerics is that a decrease of the gap with N does not necessarily imply that it vanishes in the thermodynamic limit. In particular, the gap shows a flow-reversal as function of N slightly above $\alpha_L = 0.2$, while its $N \rightarrow \infty$ value is zero only for $\alpha_L > 1/2$. In addition, we find that the gap at large α_L decays as $1/N^3$ and not $1/N^2$, which is the prediction based on \bar{A}_0 , see Eq. (19), thereby signaling the breakdown of perturbation theory. The results for the lowest non-stationary eigenvector, Fig. 16, show that it is close to a linear combination of the degenerate solutions, Eq. (17). In general, the mean-field eigenfunctions provide a fair description of the low-lying states of A within a window of eigenvalues whose extent is largest at $\alpha_L = 1$, and which decreases away from this point. At $\alpha_L = 0$ the lowest non-stationary eigenvector is almost localized on a single site.

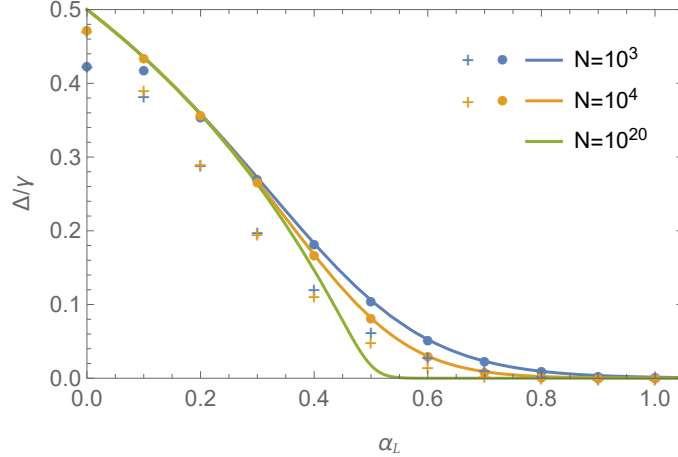


FIG. 15. The spectral gap of A_0 . The solid lines are given by Eq. (16) while the dots and crosses depict the averaged gaps (over 100 realizations) for the cases of a CPRBM and PRBM jump operator, respectively.

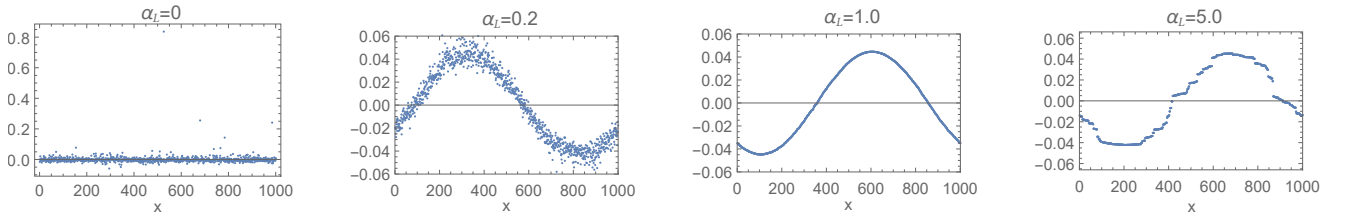


FIG. 16. Representative examples of the slowest decaying eigenvector of A_0 generated by an $N = 1000$ CPRBM jump operator.

In order to gauge the range at which the approximation of extremely localized energy-eigenstates provides a reasonable description of a PRBM system we contrast, in Fig. 17, the gap at weak decoherence calculated from A , as given

by Eq. (6), with that calculated from A_0 . The results indicate that for $\alpha_H > 3/2$ the gap is very close to that of the extreme localized system, although the gap calculated from A_0 diminishes faster with N when $\alpha_L > 1/2$. The same figure also shows that in the range $\alpha_H > 3/2$ the mode which sets the gap bears similarities to the one calculated from A_0 in terms of its envelope structure (compare with Fig. 16), although it also exhibits short range fluctuations that are absent in the latter. More importantly, we also find that in the same regime the slowest decaying mode of the full Lindbladian \mathcal{L} is largely composed of position populations and exhibits a structure that is close to that of the A_0 eigennodes, as can be seen by comparing Figs. 18 and 16.

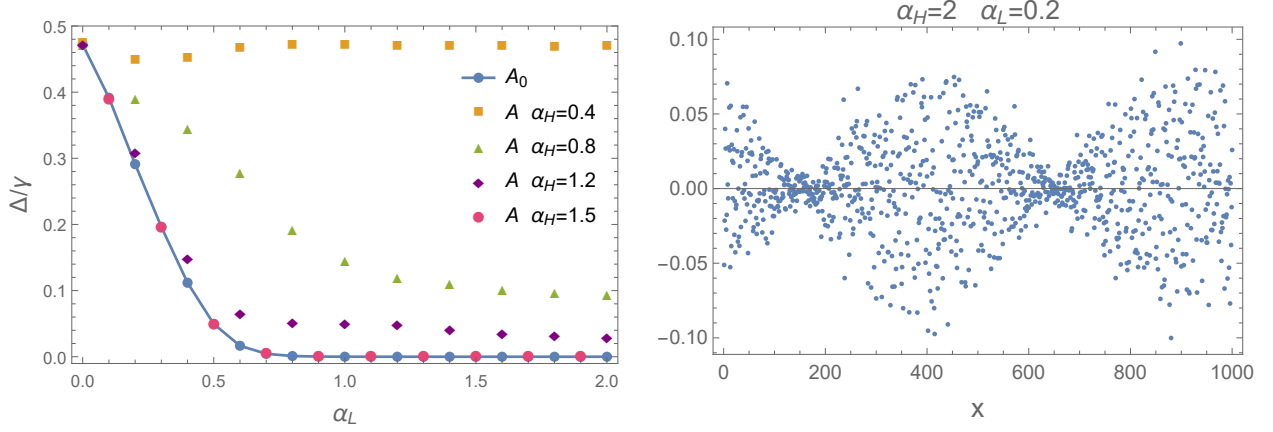


FIG. 17. Left: The spectral gap at small γ calculated from averaging over 100 realization of A with $N = 12800$ PRBM H and L , together with the gap calculated from A_0 . Right: A typical slowest decaying eigenvector of A with $N = 1000$ CPRBM, $\alpha_H = 2$ and $\alpha_L = 0.2$, shown in the x -representation.

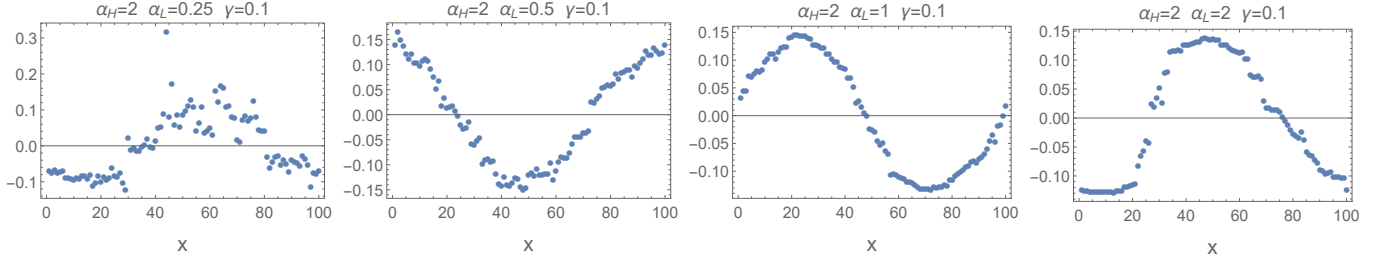


FIG. 18. Representative examples of the projection of the slowest decaying eigenvector of \mathcal{L} onto the subspace of position populations $|x\rangle\langle x|$. The data is for a system of size $N = 100$ with CPRBM H and L .

One can try to apply a similar "mean-field" analysis to understand the behavior in the range $\alpha_H > 1$, but still away from the extreme-localized regime of $\alpha_H \gg 1$. For this purpose we model the energy eigenfunctions as having an envelope with a single maximum from which it decays as $|x|^{-\alpha_H}$. This in turn implies that $U_{ij} \sim u_{ij}|P_i - j + \delta_{ij}|^{-\alpha_H}/\sqrt{a(\alpha_H, N) - 1}$, where P_i is the position of the maximum of the i th wavefunction and u_{ij} is a fluctuating amplitude of order one. Consequently, for a given H realization the average over the L_0 ensemble of the off-diagonal elements A_{ij} becomes

$$\begin{aligned}
\langle A_{ij} \rangle_L &= \left\langle \gamma \left| \sum_{mn} U_{im}(L_0)_{mn} U_{nj}^\dagger \right|^2 \right\rangle_L \\
&= \frac{\gamma}{2a(N, \alpha_L)} \sum_{mn} [(U_{im})^2 (U_{jn})^2 + U_{im} U_{jm} U_{in} U_{jn}] f_{L,mn}^2 \\
&\sim \frac{\gamma}{a(N, \alpha_L) [a(\alpha_H, N) - 1]^2} \left\{ \sum_{mn} u_{im}^2 u_{jn}^2 |P_i - m + \delta_{mP_i}|^{-2\alpha_H} |P_j - n + \delta_{nP_j}|^{-2\alpha_H} |m - n + \delta_{mn}|^{-2\alpha_L} \right. \\
&\quad \left. + \sum_{mn} u_{im} u_{jm} u_{in} u_{jn} |P_i - m + \delta_{mP_i}|^{-\alpha_H} |P_j - m + \delta_{mP_j}|^{-\alpha_H} \right. \\
&\quad \left. \times |P_i - n + \delta_{nP_i}|^{-\alpha_H} |P_j - n + \delta_{nP_j}|^{-\alpha_H} |m - n + \delta_{mn}|^{-2\alpha_L} \right\} \\
&\sim \frac{\gamma}{a(N, \alpha_L) [a(\alpha_H, N) - 1]^2} \left\{ u_{iP_i}^2 u_{jP_j}^2 |P_i - P_j|^{-2\alpha_L} + [u_{iP_i}^2 u_{jP_i}^2 + u_{iP_j}^2 u_{jP_j}^2] |P_i - P_j|^{-2\alpha_H} \right\}, \quad (21)
\end{aligned}$$

where we have assumed real U and neglected edge effects (as appropriate for CPRBM). Since we treat $\alpha_H > 1$ the sums are controlled by summands of order 1. In the first sum this occurs when $m = P_i$ and $n = P_j$ or when $m = n = P_i$ or $m = n = P_j$. The latter case also dominates the second sum. Thus, under the specified assumptions and after replacing the fluctuating u_{ij}^2 by their mean $\langle A \rangle_L$ is approximately similar to A_0 , Eq. (14), with $\alpha = \min(\alpha_H, \alpha_L)$. This in turn would imply that the gap closes for $\alpha_L > 1/2$, as we indeed find by numerically diagonalizing A . Note, however, that the N -scaling of the numerical results, Fig. 7, deviates from the expected behavior of A_0 for the corresponding α , Eq. (19), and roughly follows $N^{-(\alpha_H-1)}$ in the range of parameters that we studied. This is most likely due to our neglect of the mutual orthogonality of the energy wavefunctions, their more complicated structure, which especially in the range $3/2 > \alpha_H > 1$ often exhibits more than one peak and finally, the effects of fluctuations.

F. Small γ and $\alpha_H < 1/2$

In this range of parameters we first discuss the consequences of Eq. (6) and then indicate when and how its predictions are expected to fail in the $N \rightarrow \infty$ limit.

1. $N < \exp(4/\gamma^2)$

For $\alpha_H < 1/2$ the statistical properties of the energy eigenfunctions are close to those exhibited by the GOE. Hence, we approximate the elements of U as independent (neglecting the orthonormality conditions) normal random variables with zero mean and variance $1/N$. Under this approximation it is easy to verify that $U_{im}(L_0)_{mn} U_{nj}^\dagger$ form a set of independent random variables that obey the Lyapunov condition for the central limit theorem. Hence, as $N \rightarrow \infty$, the off-diagonal elements A_{ij} , see Eq. (21), are chi-squared distributed in the ensemble of Hamiltonians and jump operators (whose statistics we denote by the subscript LH) with mean and standard deviation

$$\begin{aligned}
\langle A_{ij} \rangle_{LH} &= \frac{\gamma}{2a(N, \alpha_L) N^2} \left[\sum_{mn} f_{L,mn}^2 + N \right] = \frac{\gamma}{2N}, \\
\sigma_{LH}(A_{ij}) &= \sqrt{2} \langle A_{ij} \rangle_{LH} = \frac{\gamma}{\sqrt{2N}}, \quad (22)
\end{aligned}$$

where we have assumed CPRBM and used $\sum_n f_{L,mn}^2 + 1 = a(N, \alpha_L) + (N/2)^{-2\alpha_L}$, which follows from Eq. (4). Consequently, owing to the central limit theorem the diagonal elements $A_{ii} = -\sum_{j \neq i} A_{ij}$ are normally distributed with slight dependence between them (L_{ij} appears both in A_{ii} and A_{jj}) and

$$\begin{aligned}
\langle A_{ii} \rangle_{LH} &= -\frac{\gamma}{2}, \\
\sigma_{LH}(A_{ii}) &= \frac{\gamma}{\sqrt{2N}}. \quad (23)
\end{aligned}$$

We have shown that such a behavior leads to a gap $\Delta = \gamma/2$ [3]. One can reach the same conclusion based on the observation that for $\alpha_H < 1/2$ the slowest decaying mode is dominated by a single H -population (see Fig. 11) for which $|A_{ii}|$ is minimal. To estimate the gap, which is close to this matrix element, consider the probability distribution of the largest value, X , among N iid random variables with Gaussian probability distribution $f_G(x)$ and cumulative distribution function $F_G(x)$

$$f_X(X) = N f_G(X) [F_G(X)]^{N-1} = \frac{N}{2^{N-1} \sqrt{2\pi\sigma^2}} e^{-\frac{(X-\mu)^2}{2\sigma^2}} \left[1 + \operatorname{erf} \left(\frac{X-\mu}{\sqrt{2}\sigma} \right) \right]^{N-1}. \quad (24)$$

Its mean can be estimated using the saddle-point approximation which up to logarithmic accuracy leads to

$$\mu(X) \approx \mu + \sigma \sqrt{2 \ln \left(\frac{N}{\sqrt{2\pi}} \right)}. \quad (25)$$

Applying this result to the diagonal elements of A implies that as $N \rightarrow \infty$ the smallest $|A_{ii}|$ resides at $-\gamma/2$.

To evaluate the perturbative correction to the gap consider the difference, u , between the two largest diagonal elements of A (the ones with smallest absolute values). Its distribution is given by

$$\begin{aligned} f_u(u) &= \int_{-\infty}^{\infty} dx N(N-1) f_G(x) f_G(x-u) [F_G(x-u)]^{N-2} \\ &= \frac{N}{2^{N-1} \sqrt{2\pi}\sigma} \int_{-\infty}^{\infty} dx \left(x + \frac{u}{\sigma} \right) e^{-\frac{1}{2} \left(x + \frac{u}{\sigma} \right)^2} \left[1 + \operatorname{erf} \left(\frac{x}{\sqrt{2}} \right) \right]^{N-1} \underset{u \ll \sigma}{\approx} \frac{1}{\sigma} \sqrt{2 \ln \left(\frac{N}{\sqrt{2\pi}} \right)}. \end{aligned} \quad (26)$$

The gap may close when the correction to the extremal eigenvalue $\sum_{j \neq i} |A_{ij}|^2 / (A_{ii} - A_{ij}) < \sum_{j \neq i} |A_{ij}|^2 / u$ becomes of order $|A_{ii}|$. Since both the distributions of A_{ii} , Eq. (23), and of $\sum_{j \neq i} |A_{ij}|^2$ (approximately normal with mean $3\gamma^2/4N$ and standard deviation $\sqrt{6}\gamma^2/N^{3/2}$) become sharp in the large N limit the condition for gap closure becomes $u < \left\langle \sum_{j \neq i} |A_{ij}|^2 \right\rangle_{LH} / \langle |A_{ii}| \rangle_{LH} \approx \gamma/N$. Since $\gamma/N \ll \sigma_{LH}(A_{ii})$ we can use Eq. (26) to find that the probability for this to happen scales as

$$P(u < \gamma/N) \approx \frac{\gamma}{N \sigma_{LH}(A_{ii})} \sqrt{2 \ln \left(\frac{N}{\sqrt{2\pi}} \right)} \sim \sqrt{\frac{\ln N}{N}}, \quad (27)$$

and thus vanishes in the large N limit.

Our numerical results, presented in Fig. 7, agree with the conclusion that $\Delta = \gamma/2$. The full Lindbladian spectrum, as presented in the main text, also points towards a gapped phase for $\alpha_H < 1/2$, despite the fact that the H -populations fail to provide an accurate description of the slowest decaying mode in the small- γ large- N limit. In particular, the mode is not dominated by a single H -population, see Fig. 11. As we argue next, this apparent gap is expected to close down in the limit $N \rightarrow \infty$, owing to rare events that occur when $\alpha_L > 1/2$.

2. $N > \exp(4/\gamma^2)$

The deduction of the Lindbladian gap from Eq. (6) is based on the assumption that in the limit of weak decoherence the lowest lying Lindbladian eigenstates originate from the H -populations, which are zero modes in the strict $\gamma = 0$ case. There is, however, another way by which a low-lying state may emerge. For this to happen, the extremal L -eigenvalue, *i.e.*, the one with the largest magnitude eigenvalue κ_{ext} , needs to obey $|\kappa_{\text{ext}}| \gg \gamma^{-1}$. Such an eigenstate may emerge for $\alpha_L > 1/2$, where the L -spectrum is unbounded. The resulting low-lying state is then adiabatically connected to the corresponding L -population $|\kappa_{\text{ext}}\rangle\langle\kappa_{\text{ext}}|$.

To see this, start from the $H = 0$ limit where $|\kappa_{\text{ext}}\rangle\langle\kappa_{\text{ext}}|$ (as all the other L -populations) is a zero mode. A non-zero Hamiltonian couples $|\kappa_{\text{ext}}\rangle\langle\kappa_{\text{ext}}|$ to L -coherences of the form $|\kappa_{\text{ext}}\rangle\langle\kappa_i|$ and $|\kappa_i\rangle\langle\kappa_{\text{ext}}|$. The latter are eigenmodes of the $H = 0$ Lindbladian with eigenvalues $-(\gamma/2)(\kappa_{\text{ext}} - \kappa_i)^2$. Consequently, second order perturbation theory leads to a shift in the eigenvalue of $|\kappa_{\text{ext}}\rangle\langle\kappa_{\text{ext}}|$ of magnitude $\Delta\lambda = -(4/\gamma) \sum_{\kappa_i \neq \kappa_{\text{ext}}} |H_{\kappa_i \kappa_{\text{ext}}}|^2 / (\kappa_{\text{ext}} - \kappa_i)^2$, where $H_{\kappa_i \kappa_j} = \langle\kappa_i|H|\kappa_j\rangle$. To make progress with estimating this sum we model the κ_i s as independent normal variables. Our

numerical calculations, presented in Fig. 19, provide evidence that this approximation is reasonable for our purposes. The numerics also indicates that the average $\langle \Delta \lambda \rangle_{LH}$ is dominated by rare events with small spacing between κ_{ext} and its neighboring eigenvalue. Such events make the average diverge with N but their proportion decrease with N , see Fig. 19. Moreover, if they occur then one should apply degenerate perturbation theory to the couplings between the pair of close eigenvalues. Doing so, which is equivalent to diagonalizing A in the form given by Eq. (7) (see Fig. 25 in Sec. II J) results in $\Delta \lambda$ that is similar to its value when the level spacing is not small.

Consequently, to estimate $\langle \Delta \lambda \rangle_{LH}$ we may assume that the main contribution to the sum comes from states in the bulk of the L -spectrum $|\kappa| \lesssim 1$. Furthermore, we break the sum into windows $1/N \ll \Delta \kappa \ll 1$ containing $n \gg 1$ levels. Each such window contributes approximately $-(4/\gamma)/(\kappa_{\text{ext}} - \bar{\kappa}_i)^2 \sum_{\kappa_i \in \Delta \kappa} |H_{\kappa_i \kappa_{\text{ext}}}|^2$. By the central limit theorem $\sum_{\kappa_i \in \Delta \kappa} |H_{\kappa_i \kappa_{\text{ext}}}|^2$ is normally distributed with mean $n \langle |H_{\kappa_i \kappa_{\text{ext}}}|^2 \rangle_{LH}$ and standard deviation $\sqrt{n} \sigma_{LH}(|H_{\kappa_i \kappa_{\text{ext}}}|^2)$. One readily finds for $i \neq j$ that $\langle |H_{\kappa_i \kappa_j}|^2 \rangle_{LH} \simeq 1/(2N)$, and in the limit of well localized L -eigenstates (large α_L)

$$\sigma_{LH}(|H_{\kappa_i \kappa_j}|^2) \sim \begin{cases} N^{-1} & \alpha_H < 1/4 \\ N^{-3/2+2\alpha_H} & 1/4 < \alpha_H < 1/2 \\ N^{-1/2} & 1/2 < \alpha_H \end{cases} . \quad (28)$$

(numerically, we find a somewhat slower decay away from the large α_L limit for $\alpha > 1/4$). Hence, the fluctuations in $\sum_{\kappa_i \in \Delta \kappa} |H_{\kappa_i \kappa_{\text{ext}}}|^2$ become negligible compared to its mean for $n > N^{\max(0, 4\alpha_H - 1)}$, as long as $\alpha_H < 1/2$. Replacing the numerator by its average we finally obtain

$$\langle \Delta \lambda \rangle_{LH} \simeq -\frac{2}{\gamma N} \sum_{\kappa_i \neq \kappa_{\text{ext}}} \left\langle \frac{1}{(\kappa_{\text{ext}} - \kappa_i)^2} \right\rangle'_L \sim -\frac{2}{\gamma} \left\langle \frac{1}{\kappa_{\text{ext}}^2} \right\rangle_L \simeq -\frac{2}{\gamma \log N}, \quad (29)$$

where $\langle \rangle'_L$ denotes the restricted mean calculated by filtering out the rare events for which the denominator is much smaller than $1/N$. In evaluating Eq. (29) we have applied Eq. (25) to get $\langle \kappa_{\text{ext}} \rangle_L \sim \sqrt{\log N}$ and checked that $\langle 1/\kappa_{\text{ext}}^2 \rangle_L = 1/[\langle \kappa_{\text{ext}} \rangle_L]^2$ for large N .

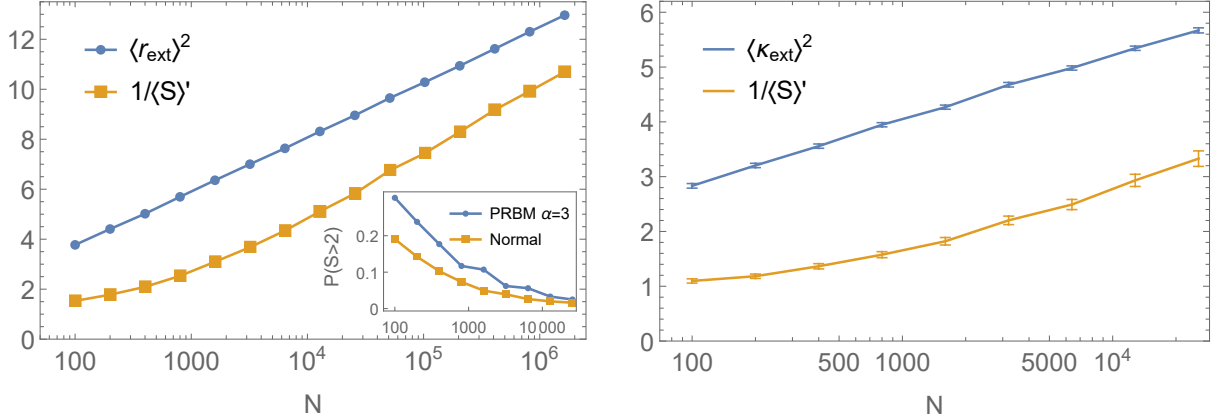


FIG. 19. Left: The (squared) mean of the extremal value r_{ext} among a sample of N normal random variables r_i with zero mean and variance $1/2$. Evidently, $\langle |r_{\text{ext}}| \rangle \sim \sqrt{\log N}$. The average of $S = (1/N) \sum_{r_i \neq r_{\text{ext}}} (r_i - r_{\text{ext}})^{-2}$ appears to diverge with N due to events with small spacing between r_{ext} and its neighbor. However, if one filters out such events by eliminating from the sample the cases for which $S > 2$ (they become rare with N , as shown by the inset) one obtains an average of S that scale approximately as $1/\log N$. Right: a similar behavior is shown by the distribution of eigenvalues of a PRBM with $\alpha = 3$.

Therefore, we conclude that for $N > e^{4/\gamma^2}$, where $|\langle \Delta \lambda \rangle_{LH}| < \gamma/2$, the gap is set by the population of the extremal L -eigenstate and follows

$$\langle \Delta \lambda \rangle_{LH} \sim \frac{1}{\gamma \log N}. \quad (30)$$

The large system sizes needed to observe the decrease of the gap with N render a direct numerical confirmation of the effect within the PRBM model impossible. Instead, we have calculated the gap in a model where the jump operator is diagonal in the x -basis with a fat-tailed distribution of eigenvalues decaying as $\nu(\kappa) \sim \kappa^{-4}$, such that

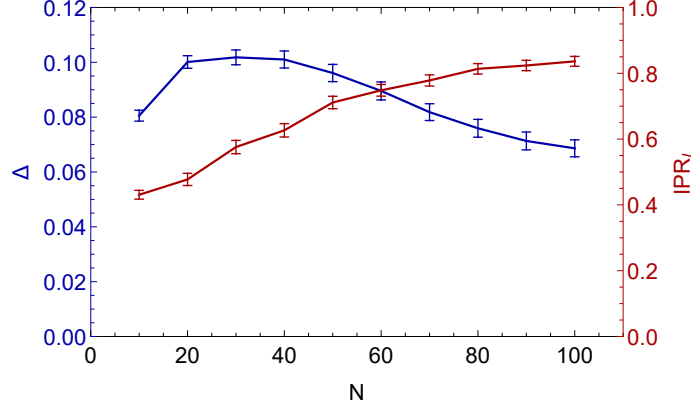


FIG. 20. The Lindbladian spectral gap and the IPR_L of the slowest decaying mode of \mathcal{L} in a system with $\gamma = 0.2$, $\alpha_H = 0$ and a jump operator whose spectrum is distributed according to $2^{13/2}/\pi(4^4 + \kappa^4)$.

its spectrum still possesses a finite variance but exhibits a more favorable scaling of the extreme eigenvalue, which approximately follows $N^{1/3}$. Fig. 20 depicts the N dependence of the gap and the IPR_L of the slowest decaying mode, and shows that at large N the gap is decreasing and set by the population of the largest L -eigenvalue.

G. Small γ and $1 > \alpha_H > 1/2$

As discussed in the main text, the H -populations fail to provide an effective description of the slowest-decaying \mathcal{L} -eigenstate when one considers the thermodynamic limit for small but fixed γ and $1 > \alpha_H > 1/2$. Here, instead, we focus on the fixed N and $\gamma \rightarrow 0$ limit where A still provides a faithful description of the asymptotic dynamics.

Fig. 11 shows that the slowest-decaying mode of A for $1 > \alpha_H > 1/2$ continues to be dominated by a single H -population - the one with the smallest $|A_{ii}|$, which approximately sets the gap. However, in contrast to the case $\alpha_H < 1/2$, where all diagonal elements of A are sharply concentrated around $-\gamma/2$, the elements associated with the localized states at the edges of the spectrum for $1 > \alpha_H > 1/2$ are much more broadly distributed. To see this, consider the mean and variance of the diagonal elements over the ensemble of L_0 . One finds,

$$\begin{aligned} \langle A_{ii} \rangle_L &= -\frac{\gamma}{2a(N, \alpha_L)} \left[a(N, \alpha_L) - 2 \sum_{mn} (U_{im})^2 (U_{in})^2 f_{L,mn}^2 \right], \\ \sigma_L^2(A_{ii}) &= \frac{\gamma^2}{2a^2(N, \alpha_L)} \sum_{mn} (U_{im})^2 (U_{in})^2 f_{L,mn}^2 \left[a(N, \alpha_L) + 1 + f_{L,mn}^2 - 8 \sum_p (U_{ip})^2 f_{L,np}^2 + 4 \sum_{pq} (U_{ip})^2 (U_{iq})^2 f_{L,pq}^2 \right]. \end{aligned} \quad (31)$$

If U follows a Porter-Thomas statistics, as outlined at the beginning of Sec. IIF, one recovers Eq. (23). The same behavior is obtained in the opposite limit of an extremely localized state with $U_{im} = \delta_{im}$, as long as $\alpha_L < 1/2$. On the other hand, for $\alpha_L > 1/2$ the above expressions lead in the large- N limit to

$$\begin{aligned} \langle A_{ii} \rangle_L &= -\frac{\zeta(2\alpha_L)}{2[1 + \zeta(2\alpha_L)]} \gamma, \\ \sigma_L(A_{ii}) &= \frac{\sqrt{\zeta(2\alpha_L)}}{2[1 + \zeta(2\alpha_L)]} \gamma. \end{aligned} \quad (32)$$

The off-diagonal elements A_{ij} that couple a localized population to the rest of the population subspace do not obey the Lyapunov condition and therefore the distribution of $A_{ii} = -\sum_{j \neq i} A_{ij}$ is not normal. Albeit, Eq. (32) indicates that it is wide with comparable mean and standard deviation. Fig. 21 demonstrates that this conclusion holds also away from the strongly localized limit and that the smallest $|A_{ii}|$ originates from populations of localized energy eigenstates. The same conclusion is reached by examining the structure of the slowest decaying mode of \mathcal{L} for a system with $N = 100$, see right panel of Fig. 21.

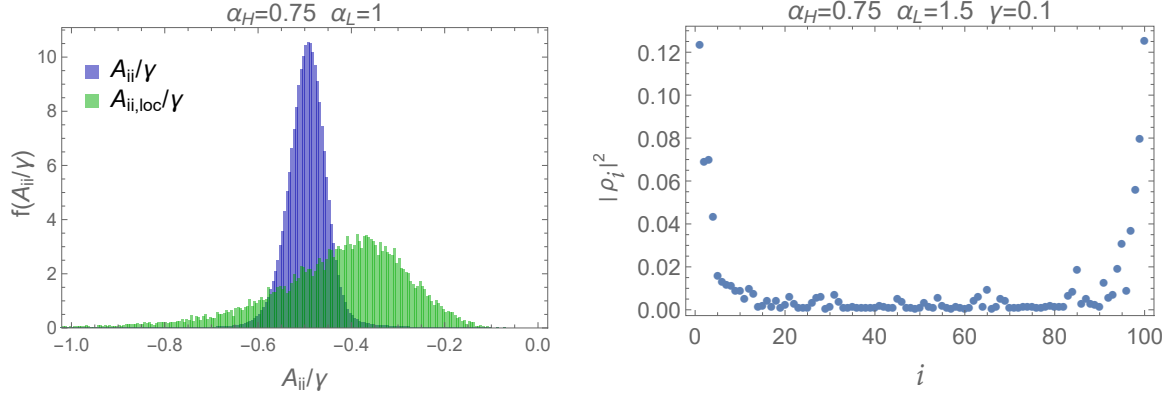


FIG. 21. Left: The distribution of all diagonal elements of A (blue) for a system with $\alpha_H = 0.75$, $\alpha_L = 1$, and $N = 1000$. In green is the distribution of the subset of diagonal elements corresponding to H -populations of energy eigenstates with $\text{IPR} > 0.1$. Right: The squared components of the projected slowest decaying \mathcal{L} -mode onto the H -population subspace $|i\rangle\langle i|$. Shown is an average over 180 realizations of a system with $N = 100$, $\gamma = 0.1$, $\alpha_H = 0.75$ and $\alpha_L = 1.5$. The H -populations are indexed according to their energies. The two maxima at the extremes of the spectrum are due to averaging. For a given realization the mode is typically concentrated near one of the edges.

Given the distribution $f_{\text{loc}}(A_{ii})$ for localized populations and its cumulative distribution function $F_{\text{loc}}(A_{ii})$ the distribution of $X = \max(A_{ii}) = \min(|A_{ii}|)$ is given by (assuming independence between the diagonal terms) $f_X(X) = n_{\text{loc}} f_{\text{loc}}(X) [F_{\text{loc}}(X)]^{n_{\text{loc}}-1}$, where n_{loc} is the number of localized energy eigenstates. Despite the fact that we are not able to calculate $f_{\text{loc}}(A_{ii})$, its breadth and the fact that n_{loc} increases with N , see Fig. 3, imply a vanishing $\langle X \rangle_{LH}$ and thus a vanishing gap for large N .

Our numerical results (Fig. 1 in the main text) indicate that the \mathcal{L} -gap also vanishes as one fixes a small γ and takes $N \rightarrow \infty$. However, in this order of limits the slowest decaying \mathcal{L} -mode ceases to be dominated by a single H -population and is delocalized both in energy and real spaces, see right panels of Figs. 11 and 12.

H. Large γ and $\alpha_L < 1/2$

Consider the eigenvalue equation for A in the $\gamma \rightarrow \infty$ limit, see Eq. (7),

$$\frac{4}{\gamma} \sum_{\substack{j=1 \\ j \neq i}}^N \left[\sum_{mn} U_{im}(H_0)_{mn} U_{jn} \right]^2 \frac{v_j - v_i}{(\kappa_j - \kappa_i)^2} = \lambda v_i, \quad (33)$$

where H_0 is the x -representation of the Hamiltonian and U is the unitary diagonalizing L . For $\alpha_L < 1/2$ the L -spectrum is largely delocalized. Approximating U as a collection of random unit vectors implies that $(H_{ij})^2 = [\sum_{mn} U_{im}(H_0)_{mn} U_{jn}]^2$ are normally distributed with $\langle |H_{ij}|^2 \rangle_{LH} = 1/2N$ and $\sigma_{LH}(\langle |H_{ij}|^2 \rangle) = 1/\sqrt{2}N$. Indexing the eigenvector components not by the L -eigenstate index but by its corresponding eigenvalue κ , and assuming that they change slowly with κ such that the arguments of Sec. II F2 allow to replace $(H_{ij})^2$ by its mean, turns Eq. (33) into

$$\frac{2}{\gamma N} P \int_{-\sqrt{2}}^{\sqrt{2}} d\kappa \nu(\kappa) \frac{v(\kappa) - v(\tau)}{(\kappa - \tau)^2} = \lambda v(\tau), \quad (34)$$

where P stands for the principle value of the integral and the $\nu(\kappa)$ is the semicircle distribution of the L -states

$$\nu(\kappa) = \frac{N}{\pi} \sqrt{2 - \kappa^2} \Theta(2 - \kappa^2). \quad (35)$$

The solutions to Eq. (34) take the form [3]

$$\lambda_n = -\frac{2}{\gamma} n, \quad v_n(\kappa) = U_n \left(\frac{\kappa}{\sqrt{2}} \right), \quad n = 0, 1, 2, \dots \quad (36)$$

where $U_n(x)$ are the Chebyshev polynomials of the second kind.

The lowest-lying state near $2/\gamma$ is clearly visible in the A -DOS presented in Fig. 14, where it also shows up with a somewhat smaller eigenvalue in the DOS of the full Lindbladian. We find that more of the discrete states, Eq. (36), appear in the A -spectrum as N is increased, see Fig. 22. Our results suggest that this also holds for the \mathcal{L} -spectrum, especially when γ is increased as well. More directly, the inset of Fig. 23 shows that the projected lowest-lying \mathcal{L} -mode for $\alpha_L < 1/2$ is approximately linear in the L -eigenvalue of the populations, as predicted by Eq. (36).

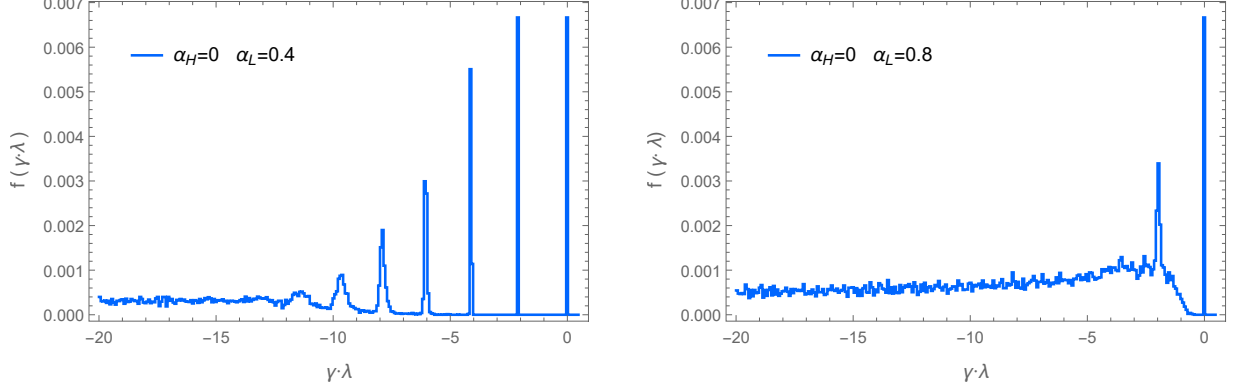


FIG. 22. Probability density of the eigenvalues of A for $\gamma \rightarrow \infty$ with $N = 2000$ averaged over 1000 realizations.

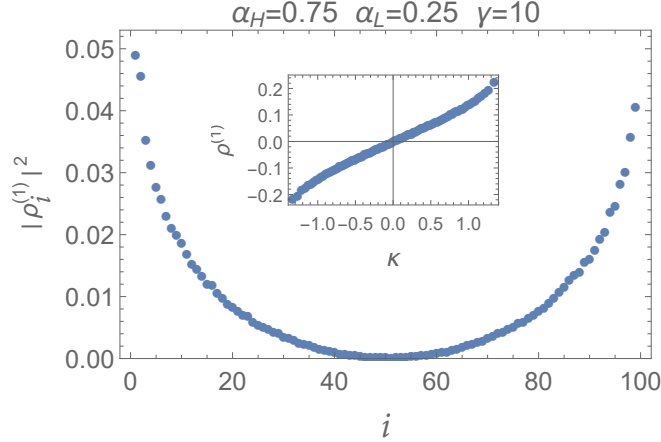


FIG. 23. The squared components of the projected slowest decaying \mathcal{L} -mode onto the L -population subspace $|i\rangle\langle i|$. Shown is an average over 180 realizations of systems with $N = 100$, $\gamma = 10$. The L -populations are indexed according to their L -eigenvalues. The inset depicts the mode components as function of the L -eigenvalue κ of the populations.

I. Large γ and $1 > \alpha_L > 1/2$

The numerical results, Fig. 8, show that in this range the spectral gap of A decreases very slowly with N . Concomitantly, the discrete low-lying states that exist in the DOS at smaller values of α_L are largely smeared out and spectral weight appears closer to the origin. This is evident in both the A -DOS and \mathcal{L} -DOS at relatively small values of N , see Fig. 14, but is particularly clear in the A -DOS for the larger values of N , as shown in Fig. 22. The mode which sets the gap becomes localized both in the L -populations subspace and in real space, see Fig. 6. It is dominated by the extremal eigenstates of L , as shown by Fig. 24.

Since the bulk of the L -spectrum is delocalized both the mean and standard deviation of the Hamiltonian elements in the L -basis scale approximately with N^{-1} , for all α_H . Hence, we may apply the analysis of Sec. II F2 and conclude

that the gap is expected to follow Eq. (30). The difference is that now it suffices to have $\log N > 1$ in order for the eigenvalue of the localized mode to reside below the one produced by the extended mode, Eq. (36).

The results that we present in the main text give evidence that the above discussion holds also for the spectrum of the full Lindbladian in the limit of large but fixed γ and $N \rightarrow \infty$, as long as $\alpha_H < 1/2$. However, the population dynamics fails to describe this limit in the range $\alpha_H > 1/2$, where the slowest-decaying modes are hydrodynamical.

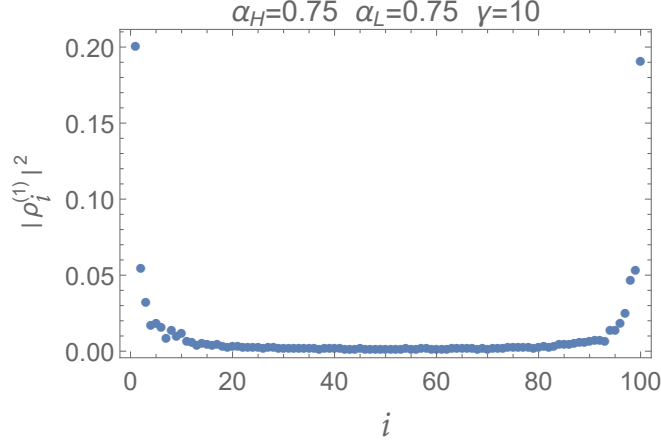


FIG. 24. The squared components of the projected slowest decaying \mathcal{L} -mode onto the L -population subspace $|i\rangle\langle i|$. Shown is an average over 180 realizations of systems with $N = 100$, $\gamma = 10$. The L -populations are indexed according to their L -eigenvalues. The two maxima at the extremes of the spectrum are due to averaging. For a given realization the mode is typically concentrated near one of the edges.

J. Large γ and $\alpha_L > 1$

When $\alpha_L > 1$ the L -spectrum is unbounded and localized. If, in addition, $\alpha_H < 1/2$, we may apply the analysis of Sec. II F2. Hence, one expects to find in this range of parameters a gap that decreases logarithmically with N according to Eq. (30) and whose corresponding mode is comprised of the extremal L -population. These expectations are indeed borne out by the numerics.

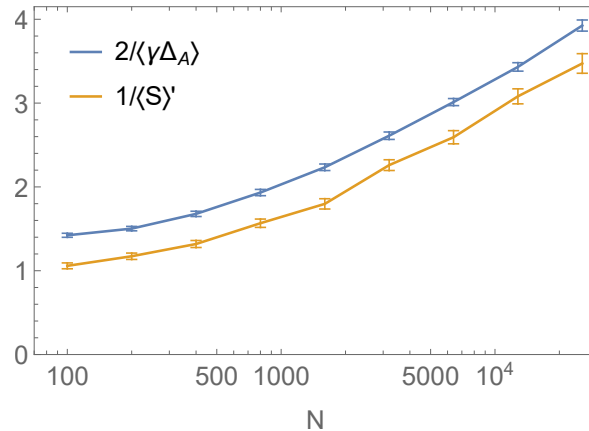


FIG. 25. The inverse of the A -gap for $\gamma \rightarrow \infty$ and $\alpha_H = 0$, $\alpha_L = 3$. Also shown is the inverse mean of $S = \min[(1/N) \sum_{i \neq 1} (\kappa_i - \kappa_1)^{-2}, (1/N) \sum_{i \neq N} (\kappa_i - \kappa_N)^{-2}]$, for the same parameters. Here, κ_1 and κ_N are the smallest (most negative) and largest L -eigenvalues. When calculating the average of S we filtered out events with $S > 2$.

Figure 25 shows that the A -gap follows the sum of inverse square spacings $\sum_{\kappa_i \neq \kappa_{\text{ext}}} (\kappa_i - \kappa_{\text{ext}})^{-2}$ (where here κ_{ext} is either the most negative or the most positive L -eigenvalue), in accord with Eq. (29). Concomitantly, Fig. 26

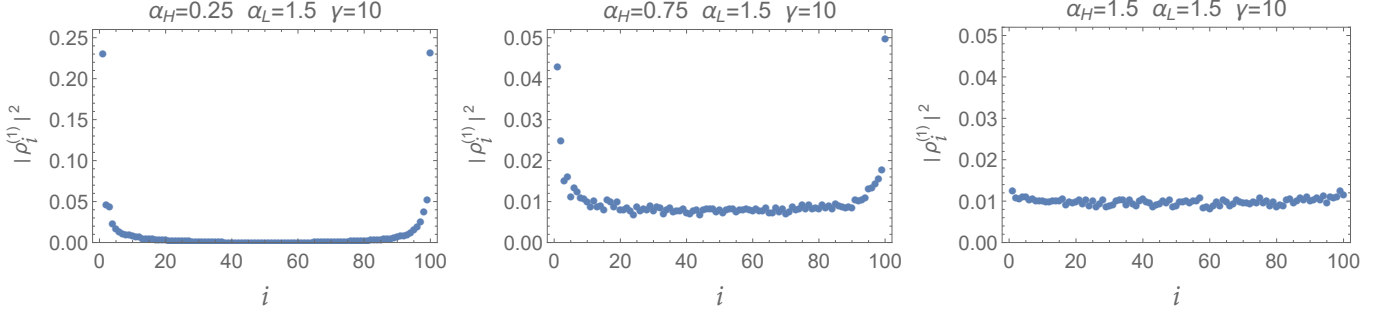


FIG. 26. The squared components of the projected slowest decaying \mathcal{L} -mode onto the L -population subspace $|i\rangle\langle i|$, averaged over 180 realizations of systems with $N = 100$, $\gamma = 10$.

shows that for $\alpha_H < 1/2$ the slowest decaying mode, not just of the effective population dynamics A , but of the full Lindbladian is given approximately by the population of the extremal L -eigenstate. The same figure also demonstrates that for $\alpha_H > 1/2$ the nature of the slowest decaying \mathcal{L} -mode changes and becomes hydrodynamic. We note that this stands in contrast to the slowest decaying eigenstate of A in the $\gamma \rightarrow \infty$ limit, which changes from being localized on the extremal L -population to being extended only when $\alpha_L > 3$ and $\alpha_H > 3/2$ (or when $\alpha_L > 3/2$ and $\alpha_H > 1/2$ for the case of the regularized A , Eq. (7), as shown by Fig. 11).

III. MULTIPLE JUMP OPERATORS

Finally, we would like to consider the way by which our results for the case of a single jump operator generalize to systems with multiple jump operators. To this end, consider the Lindblad master equation

$$\partial_t \rho = \mathcal{L}\rho \equiv -i[H, \rho] + \sum_{k=1}^{n_c} \gamma_k \left[L_k \rho L_k - \frac{1}{2} \{L_k^2, \rho\} \right], \quad (37)$$

where we have specialized to Hermitian L_k , each described by a PRBM governed by an exponent α_{L_k} . The number of noise channels n_c can run up to $N^2 - 1$.

In the limit where $\sum_k \gamma_k \ll 1$ the effects of individual decoherence channels add up, and each channel can be analyzed in a similar manner to the case of a single jump operator (Sec. II E - II G). Consequently, if we denote $\tilde{\alpha}_L = \min(\alpha_{L_k})$, the perturbative and numerical analysis yields a gapless hydrodynamic phase for $\alpha_H > 1/2$ and $\tilde{\alpha}_L > 1/2$. It predicts a gapped phase in the remaining part of the α_H - $\tilde{\alpha}_L$ plane. However, as we argue below, this conclusion fails in the range $\alpha_H < 1/2$ and $\tilde{\alpha}_L > 1/2$ where the system exhibits a weakly gapless Lifshitz phase as $N \rightarrow \infty$.

The limit of strong decoherence is complicated by the fact that the jump operators generally do not commute. Analytical progress can be made in the case where a single channel is much stronger than the others, i.e., $\gamma_1 \gg 1$, and $\gamma_1 \gg \gamma_k$ for $k = 2, \dots, n_c$. In this context, we concentrate on the case $n_c = 2$ and consider the L_1 -populations dynamics. The generalization to larger number of channels is straightforward. If one turns off the unitary dynamics, namely sets $H = 0$, the analysis proceeds exactly along the lines of Sec. II E - II G, with the only difference being that the A matrix, Eq. (6), is expressed in terms of matrix elements of L_2 in the eigenbasis of L_1 instead of H . Borrowing the corresponding conclusions we expect to find a gapped phase when $\tilde{\alpha}_L < 1/2$ and a gapless hydrodynamic phase for $\tilde{\alpha}_L > 1/2$.

We now reintroduce H and take into account its effects on the L_1 -populations dynamics, as expressed by Eq. (7). Hence, we end up with an effective A which is the sum of Eqs. (6) and (7). Both parts lead to a gapped phase for $\tilde{\alpha}_L < 1/2$ and a gapless hydrodynamic phase when $\alpha_H > 1/2$ and $\tilde{\alpha}_L > 1/2$. However, following the discussion of Sec. III - II J, we conclude that the H -induced part of A leads to a Lifshitz phase for $\alpha_H < 1/2$ and $\alpha_{L_1} > 1/2$. We have checked numerically that this conclusion remains valid when the effects of both H and L_2 are included in A , as seen in Fig. 27. Consequently, the arguments presented in Sec. II F imply that a system with $\alpha_H < 1/2$ and $\tilde{\alpha}_L > 1/2$ is expected to exhibit a gapless Lifshitz phase also for small γ_1 (and γ_2) when $N \rightarrow \infty$.

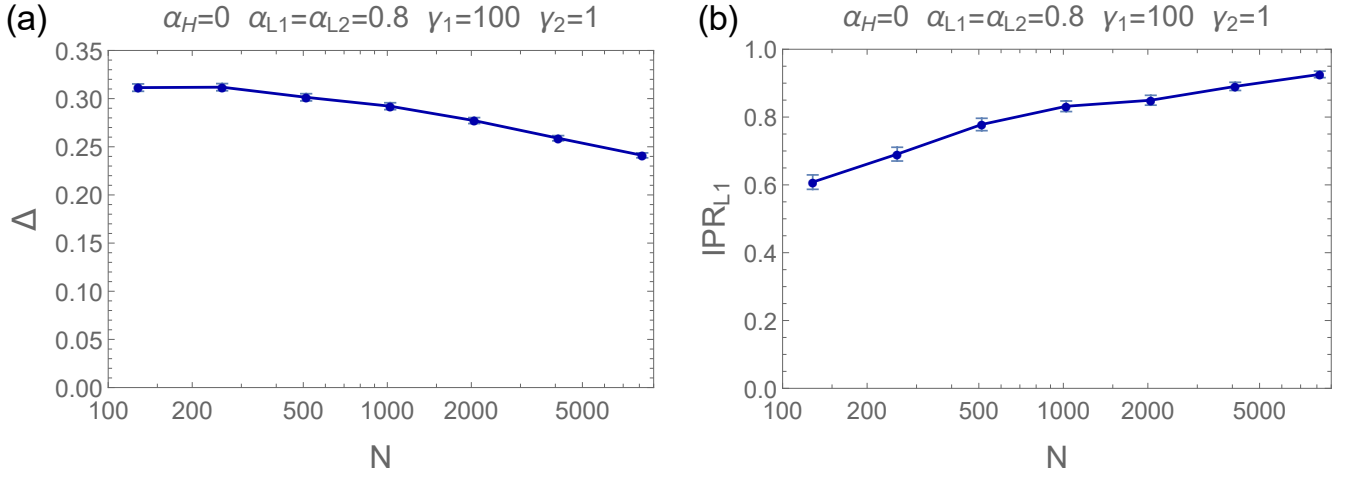


FIG. 27. (a) The spectral gap calculated from the effective dynamics of the L_1 -populations (the A matrix) for a system with a Hamiltonian and two jump operators. (b) The IPR in the L_1 basis of the slowest decaying mode.

Next, we contrast the above conclusions, based on perturbative analysis of the effective population dynamics expressed via the A matrix, with the spectrum of the full Lindbladian. We begin by considering the case of two jump operators with $\gamma_1 = \gamma_2 = \gamma$. The results, depicted in Fig. 28, exhibit the expected behavior, namely, for small γ the spectrum appears gapless when $\alpha_H > 1/2$ and $\tilde{\alpha}_L > 1/2$ and gapped otherwise. For large γ the system appears gapless when $\tilde{\alpha}_L > 1/2$ and gapped otherwise.

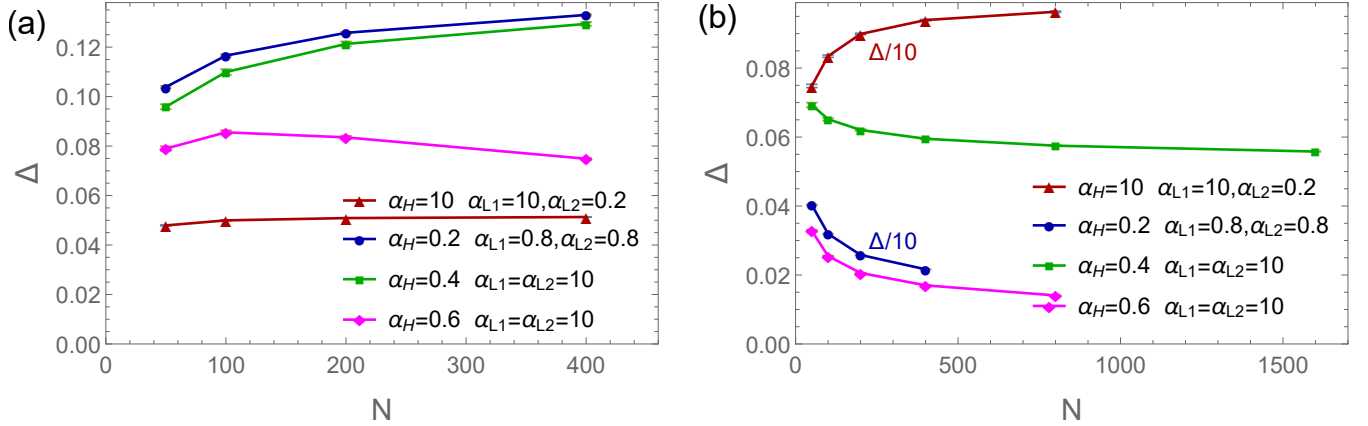


FIG. 28. (a) The Lindbladian spectral gap as a function of system size for the case of two Hermitian PRBM jump operators at weak coupling $\gamma_1 = \gamma_2 = 0.2$. Results are shown for four systems with the specified values for the exponents α_H and α_{L_1} , α_{L_2} . (b) The spectral gap of the same systems as a function of N at strong coupling $\gamma_1 = \gamma_2 = 10$.

In an effort to elucidate the nature of the gapless phase for strong decoherence, we follow the strategy outline above and treat first the model of two jump operators and no Hamiltonian ($\gamma = \infty$). The results, depicted in Fig. 29 show that: a) When $\gamma_1 = \gamma_2$ (away from the perturbative limit $\gamma_1 \gg \gamma_2$ considered above) the slowest decaying Lindbladian eigenstate largely resides in x -basis populations subspace, at least for $\tilde{\alpha}_L > 1/2$. b) The system is gapped when $\tilde{\alpha}_L < 1/2$ and gapless for $\tilde{\alpha}_L > 1/2$, and c) The slowest decaying mode is hydrodynamic.

Consequently, we add the Hamiltonian and concentrate on the character of the slowest decaying mode in the gapless phase $\tilde{\alpha}_L > 1/2$. We begin by considering the simpler case, where the two jump operators commute. Specifically, when they are diagonal in the x -basis with matrix elements that are given by the eigenvalues of two $\alpha = 10$ PRBMs (and are therefore unbound). Fig. 30 shows that while the spectral gap slowly decays with N for both $\alpha_H < 1/2$ and for $\alpha_H > 1/2$, the corresponding mode is localized in real space (Lifshitz phase) in the former case and delocalized (hydrodynamical phase) in the latter.

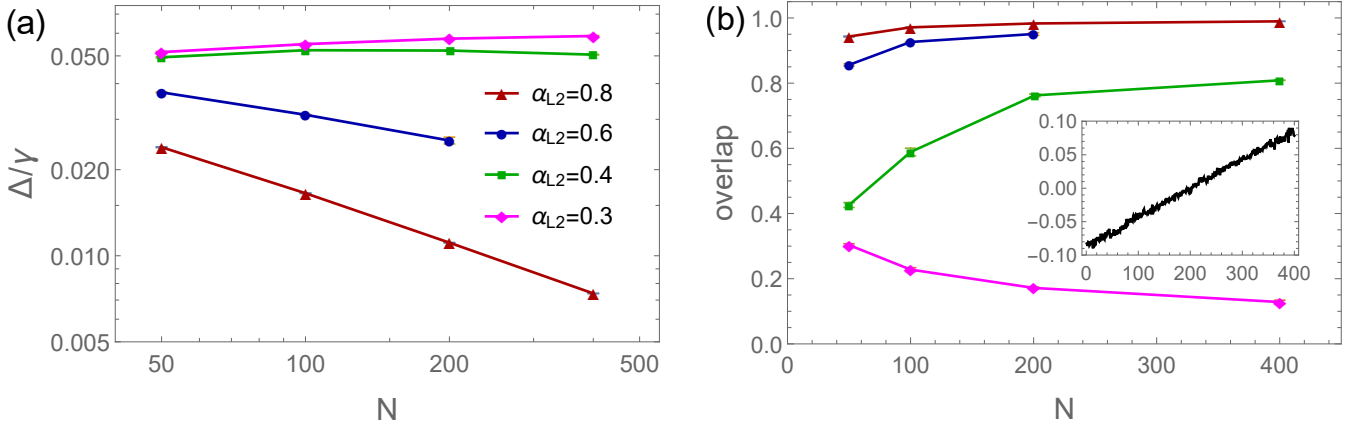


FIG. 29. (a) The Lindbladian spectral gap as a function of system size for the case of pure noisy dynamics ($H = 0$) with two Hermitian PRBM jump operators. The results are for systems with $\alpha_{L1} = 0.8$, $\gamma_1 = \gamma_2 = \gamma$ and various values of α_{L2} . (b) The overlap of the slowest decaying mode with the x -basis populations in the same systems. The inset depicts a representative example of the slowest mode for $\alpha_{L2} = 0.4$. Shown are its components in the subspace of x -basis populations.

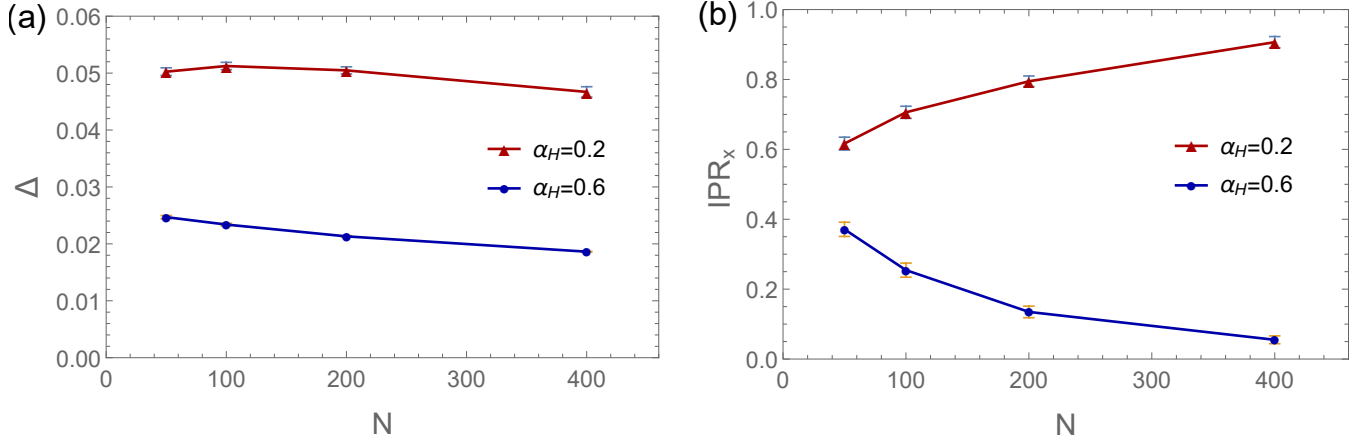


FIG. 30. (a) The Lindbladian spectral gap as a function of system size for the case of two jump operators that are diagonal in the x -basis. Their diagonal elements are random permutations of the eigenvalues of two $\alpha = 10$ PRBMs. The system is at strong coupling $\gamma_1 = \gamma_2 = 10$, and its Hamiltonian is a PRBM with the specified values for α_H . (b) The IPR in the x -basis of the slowest decaying eigenstate of the same systems.

To further establish the existence of a Lifshitz phase in the regime $\alpha_H < 1/2$ and $\tilde{\alpha}_L > 1/2$ we turn to the more general case, where the two jump operators do not commute. Fig. 31 provides evidence that the Lifshitz phase survives in this case as well. Specifically, it follows the slowest decaying mode in a system with $\alpha_H = 0$ and two Hermitian PRBM jump operators with $\alpha_{L1} = \alpha_{L2} = 0.8$ or 1.2 , as γ_2 is increased towards $\gamma_1 = 10$. The findings for the limit $\gamma_2 = 0$ agree with our previous results. We observe a gap that begins to decay slowly at large N (at least for $\alpha_L = 1.2$, although not yet for $\alpha_L = 0.8$) with a concomitant increase of the real-space IPR - both indicative of a Lifshitz mode. As γ_2 increases the rise in the IPR commences at larger values of N . However, the fact that we observe the localization of the mode for $\gamma_2 = 3$ (and perhaps also for $\gamma_2 = 5$ in the $\alpha_L = 1.2$ system) leads us to believe that the Lifshitz phase is established when $N \rightarrow \infty$ even for $\gamma_2 = \gamma_1$. This conclusion is supported by our observation, see Fig. 32, of Lifshitz behavior for $\gamma_1 = \gamma_2$, when $\alpha_{L1} = \alpha_{L2} = 10$, i.e., when the non-commutativity of the jump operators is still present but weaker.

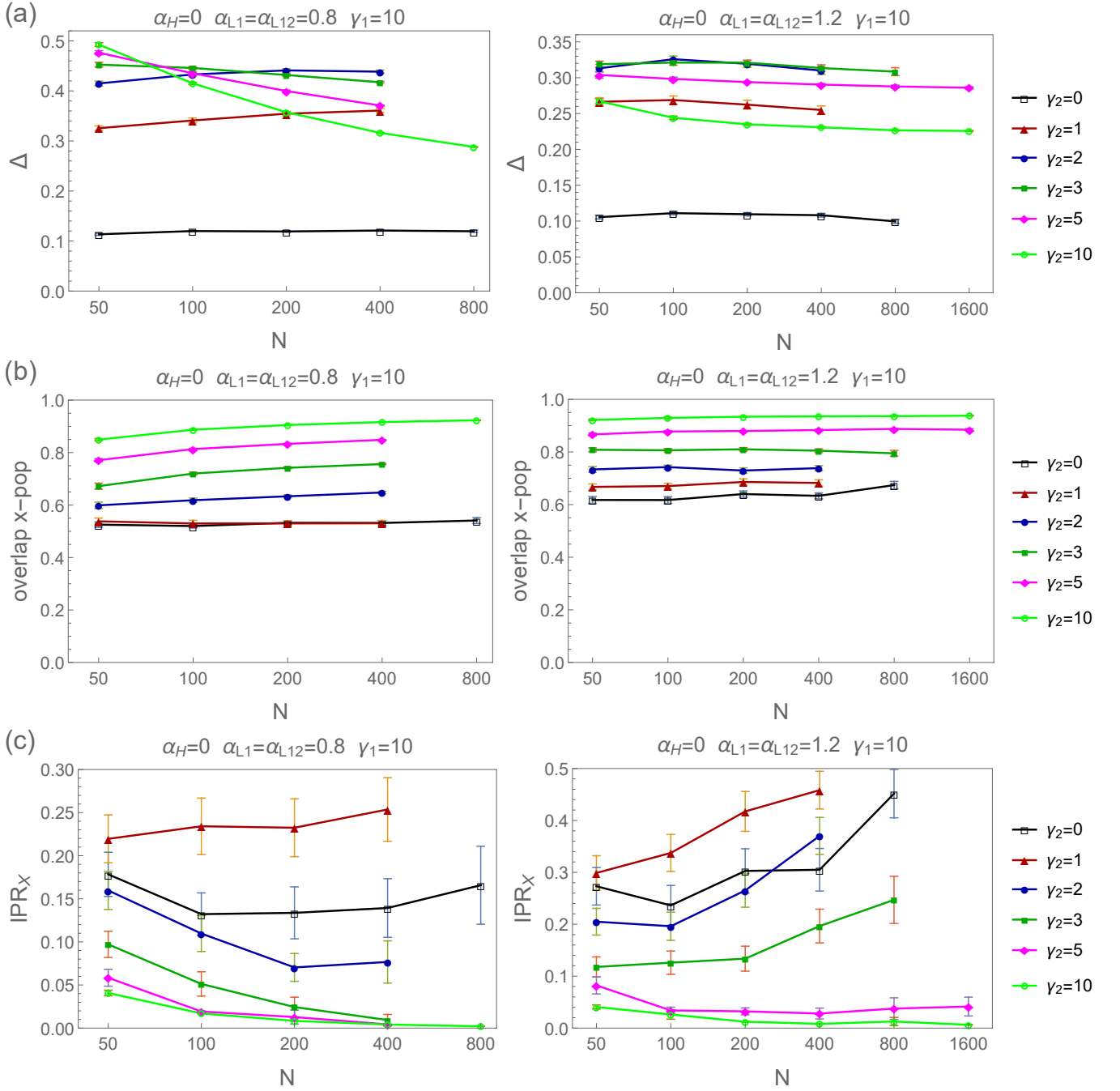


FIG. 31. The case of a Hamiltonian with $\alpha_H = 0$ and two Hermitian PRBM jump operators with $\alpha_{L1} = \alpha_{L2} = 0.8$ (left), and $\alpha_{L1} = \alpha_{L2} = 1.2$ (right). The results are for systems with $\gamma_1 = 10$ and various values of γ_2 , as indicated. The figure depicts the dependence on system size for (a) The Lindbladian spectral gap, (b) The overlap of the slowest decaying Lindbladian mode with the subspace of x -basis populations, and (c) The IPR_X of the slowest decaying Lindbladian mode.

Finally, we briefly turn to the case of many jump operators. Fig. 33 considers the case where a system of size N is coupled to the environment via N jump operators, each localized on a different site. When the couplings are taken from a distribution of an $\alpha = 10$ PRBM (which is therefore unbound), we again find a transition from a localized Lifshitz phase to a delocalized hydrodynamic phase as α_H increases beyond $1/2$. Fig. 34 demonstrates that it suffices to add to the system a single jump operator with $\alpha_L < 1/2$ in order to establish a spectral gap. This provides further support to our claim for a gapped phase whenever $\tilde{\alpha}_L < 1/2$.

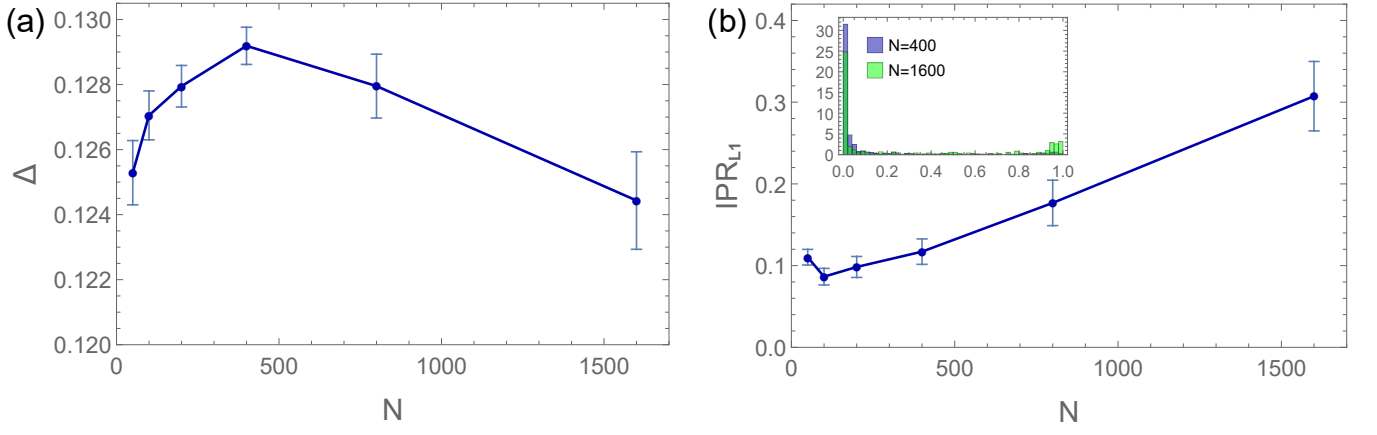


FIG. 32. (a) The Lindbladian spectral gap as a function of system size for the case of two Hermitian PRBM jump operators with $\alpha_{L_1} = \alpha_{L_2} = 10$ and a Hamiltonian with $\alpha_H = 0.2$, at strong coupling $\gamma_1 = \gamma_2 = 10$. (b) The IPR of the slowest decaying mode in the basis of the L_1 eigenfunctions. The inset depicts the distribution function of the IPR for $N = 400$ and $N = 1600$.

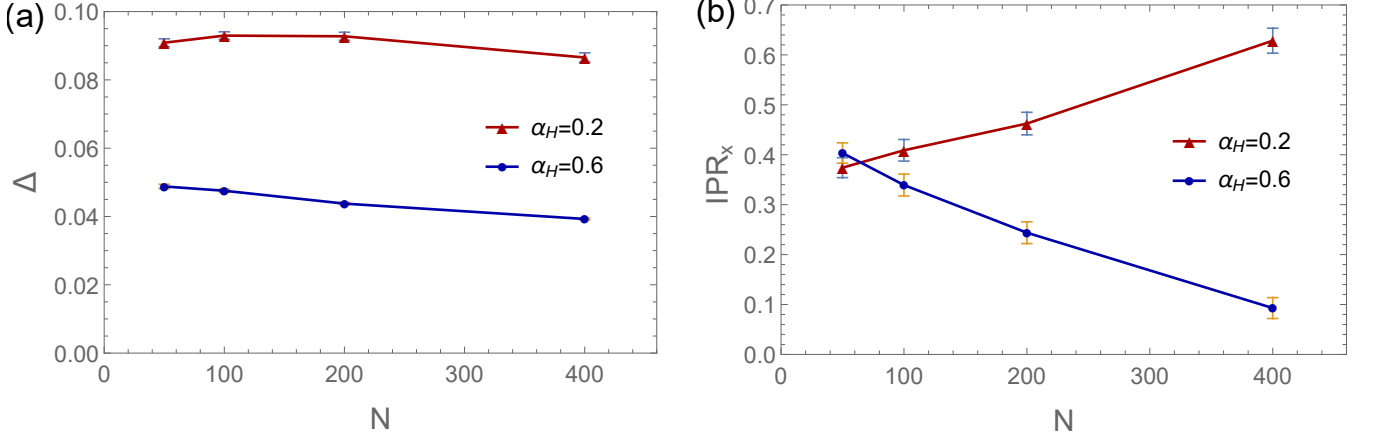


FIG. 33. (a) The Lindbladian spectral gap as a function of system size for the case of N jump operators, each localized on a different site. Their strengths are taken from a random permutation of the eigenvalues of an $\alpha = 10$ PRBM. The system is at strong coupling $\gamma_k = 10$, and its Hamiltonian is a PRBM with the specified values for α_H . (b) The IPR in the x -basis of the slowest decaying eigenstate of the same systems.

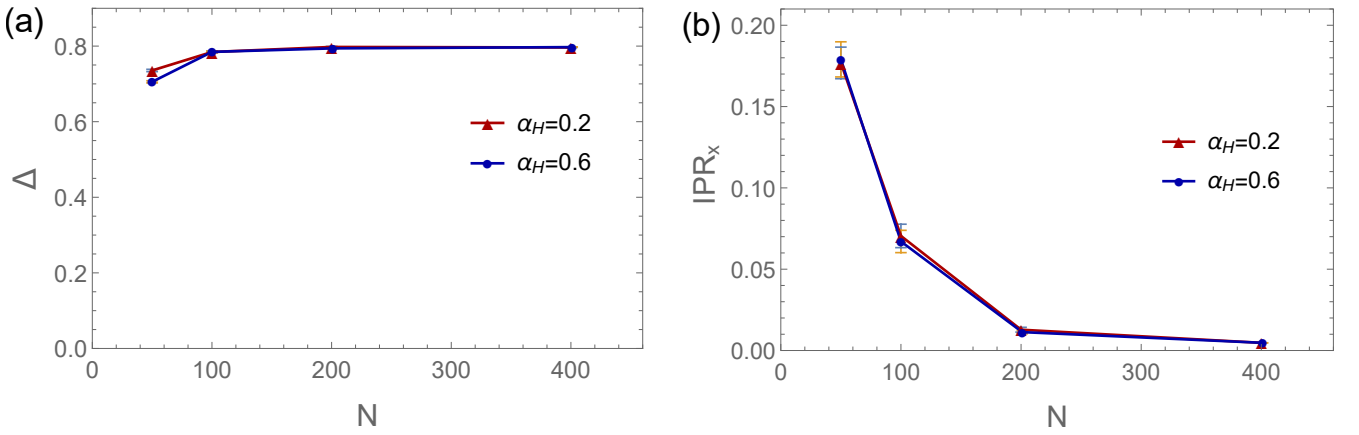


FIG. 34. Same as Fig. 33 with an additional jump operator that is a PRBM in the x -basis with $\alpha_L = 0.3$.

IV. DYNAMICS OF LOCAL OBSERVABLES

To tie the discussion of the Lindbladian gap Δ to the time dependence of local observables we have calculated the evolution of an initial state of the form

$$\rho_{ij}(t=0) = \begin{cases} 0 & i = j = 1 \\ \frac{1}{N-1} & i = j \neq 1 \\ 0 & i \neq j \end{cases} . \quad (38)$$

We have fitted the diagonal elements $\rho_{ii}(t)$ (see examples in Figs. 37 and 39) to an exponential relaxation over different time windows, thereby extracting the relaxation rate $1/\tau$. The results for the limit of strong decoherence appear in Fig. 3 of the main text, and the results for weak decoherence are depicted here in Fig. 35. In both cases, we find an asymptotic exponential relaxation of the local observable ρ_{ii} with an asymptotic relaxation rate that equals the gap. However, for each ρ_{ii} the asymptotic relaxation commences at a different time, as demonstrated by Figs. 37 and 39. This time correlates with the overlap between $\rho_{ii}(t=0)$ and the Lindbladian slowest relaxing mode ρ_1 . Smaller overlap implies a later onset of the asymptotic relaxation. This is shown by Figs. 36 and 38 that present the relative difference $(\tau^{-1} - \Delta)/\Delta$ between the relaxation rate extracted from the range $t = 9 - 12\Delta^{-1}$ and the gap.

We find that the asymptotic relaxation starts early (in terms of the natural time scale Δ^{-1}) in the hydrodynamic phase, both in the limits of large and small γ . In addition, it exhibits small fluctuations in the onset time of the asymptotic relaxation due to the smooth nature of the hydrodynamic modes. The final approach to the steady state starts later in the gapped phase. In the strong decoherence limit it also exhibits larger fluctuations, due to the random nature of ρ_1 , while the more regular structure of ρ_1 in the limit of small γ (at least for large α_H , see Sec. II E) implies smaller fluctuations in the onset time, see Figs. 36 and 38. Finally, we find that in the Lifshitz phase the time where the dynamics starts being controlled by the gap is the longest. This behavior is accompanied by large fluctuations in the onset time. Both of these features find their origin in the nature of ρ_1 that tends to be highly localized with only an algebraically-small overlap with the majority of sites in the system.

In conclusion, let us comment about the dependence of the onset time on the system size. As N grows, the number of slowly-relaxing Lindbladian eigenstates near ρ_1 increases as well. This is particularly true for the gapped phase in the limit of small γ , where the spectral width of the entire cloud of \mathcal{L} -eigenvalues along the real axis does not scale with N and is of order γ . Therefore the late-time dynamics involves many close spaced eigenstates, and it is difficult to isolate the truly asymptotic relaxation due to ρ_1 . Nevertheless, the same reason also implies that the relaxation necessarily takes place on the time scale Δ^{-1} .

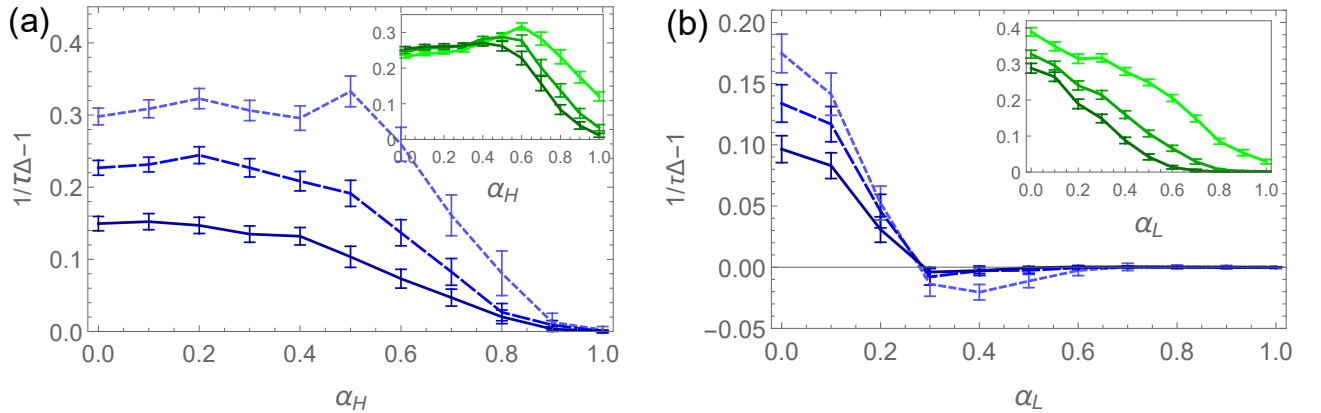


FIG. 35. (a) The relative difference between the spatial average of the relaxation rate τ^{-1} of local observables and Δ for $\gamma = 0.2$, $\alpha_L = 1.5$ and $N = 100$. The dotted, dashed and solid lines are based on τ extracted by fitting the relaxation over the range $t = 3 - 6$, $6 - 9$ and $9 - 12\Delta^{-1}$, respectively. The inset shows the standard deviation of the relative difference. (b) The same quantities as a function of α_L for $\alpha_H = 1.5$.

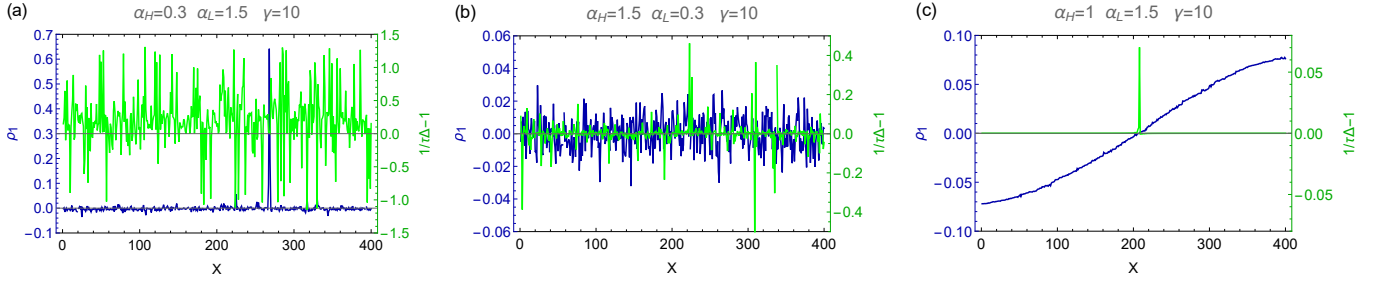


FIG. 36. Representative examples of the slowest relaxing mode ρ_1 (blue) and the relative difference between the relaxation rate τ^{-1} of the local observables and Δ (green) for a system with $\gamma = 10$, $N = 400$. τ was extracted for each site by fitting the relaxation of ρ_{ii} over the range $t = 9 - 12\Delta^{-1}$. Results are shown for (a) the Lifshitz phase, (b) the gapped phase, and (c) the hydrodynamic phase.

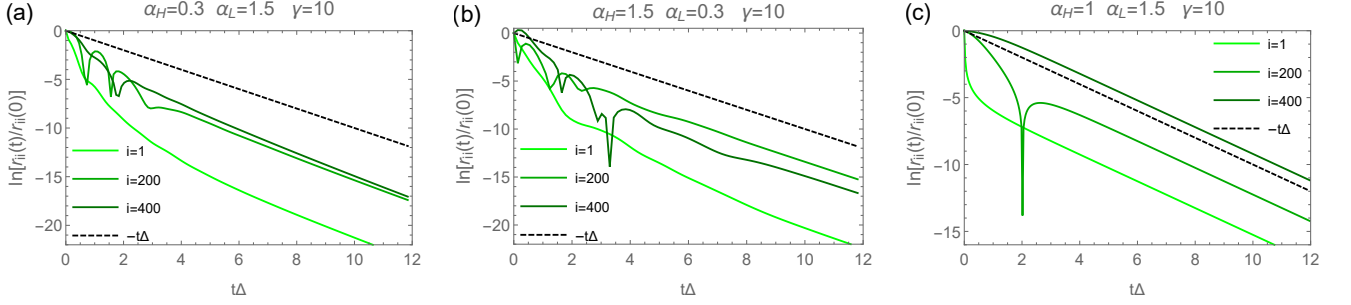


FIG. 37. The time evolution of $r_{ii} = |\rho_{ii} - 1/N|$ on sites $i = 1, 200$ and 400 in the samples presented in Fig. 36.

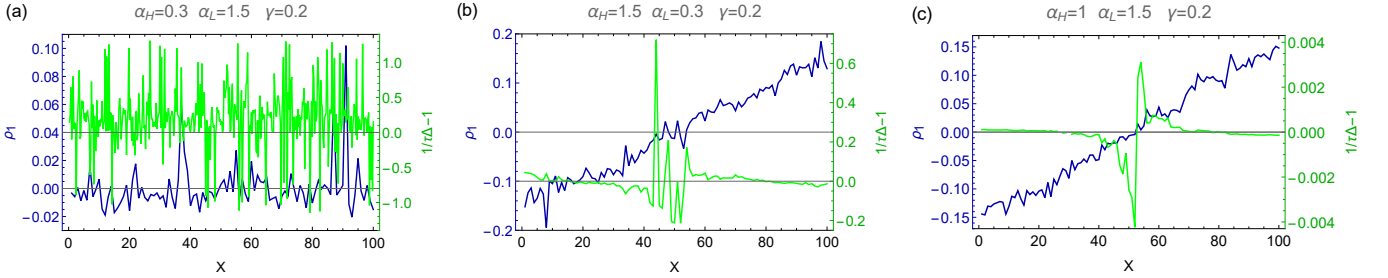


FIG. 38. Representative examples of the slowest relaxing mode ρ_1 (blue) and the relative difference between the relaxation rate τ^{-1} of the local observables and Δ (green) for a system with $\gamma = 0.2$, $N = 100$. τ was extracted for each site by fitting the relaxation of ρ_{ii} over the range $t = 9 - 12\Delta^{-1}$. Results are shown for (a) the Lifshitz phase (whose expected behavior is still not apparent for this system size), (b) the gapped phase, and (c) the hydrodynamic phase.

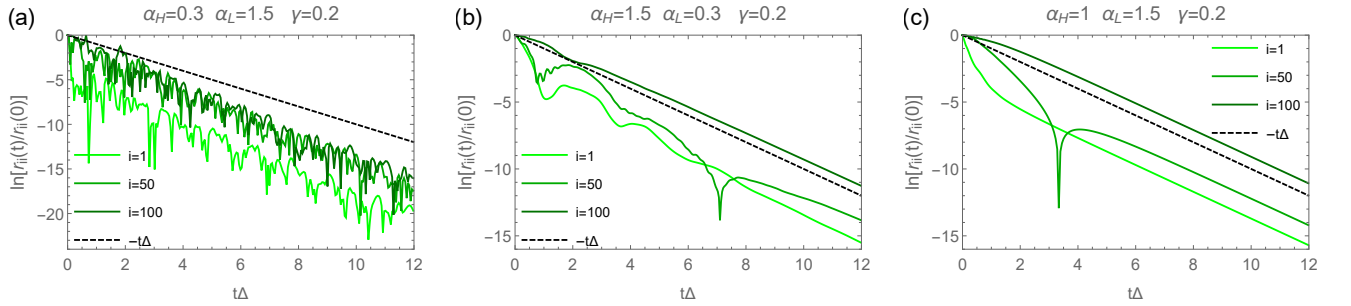


FIG. 39. The time evolution of $r_{ii} = |\rho_{ii} - 1/N|$ on sites $i = 1, 50$ and 100 in the samples presented in Fig. 38.

-
- [1] A. D. Mirlin, Y. V. Fyodorov, F.-M. Dittes, J. Quezada, and T. H. Seligman, "Transition from localized to extended eigenstates in the ensemble of power-law random banded matrices", Phys. Rev. E **54**, 3221, (1996).
 - [2] O. Yevtushenko and V. E. Kravtsov, "Density of states for almost-diagonal random matrices", Phys. Rev. E **69**, 026104 (2004).
 - [3] T. Can, V. Oganessian, D. Orgad and S. Gopalakrishnan, "Spectral gaps and midgap states in random quantum master equations", Phys. Rev. Lett. **123**, 234103 (2019).